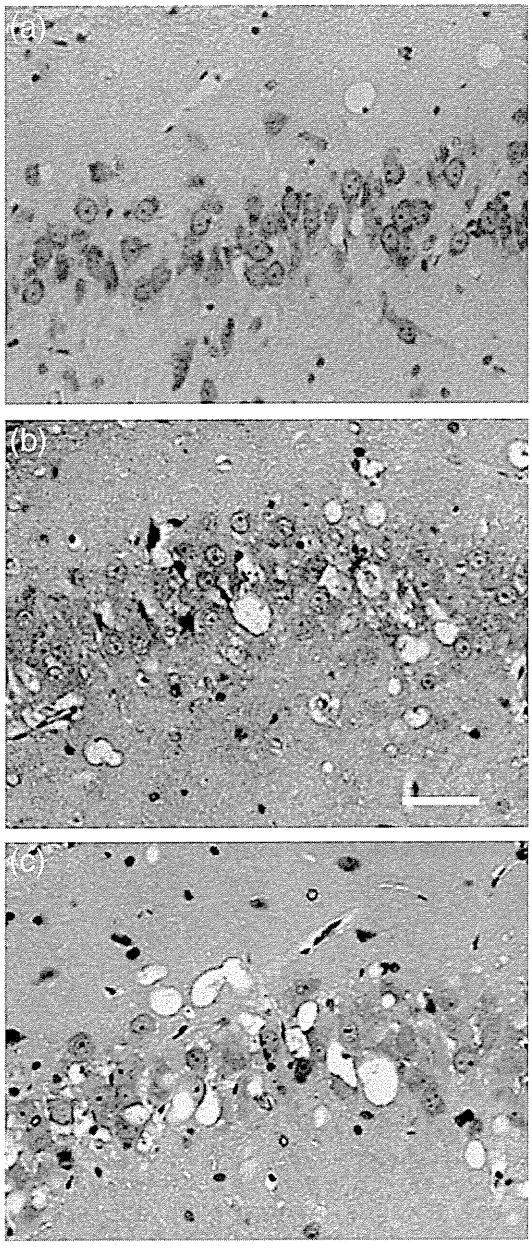

Fig. 6 – Immunohistostaining of CA3 neurons in mature spontaneously epileptic rats (SER). Immunoreactive neurons to TUNEL (a), bax (b), or caspase-3- (c) were not found. The scale bar represents 50 μm.

Hippocampal CA3 neurons of SER were vulnerable because of the voltage-dependent calcium channel abnormality (Yan et al., 2007). Ca^{2+} influx of the SER hippocampus induced by MF stimulation was observed in CA2 (along the trisynaptic pathway), although Ca^{2+} influx in CA1 was limited (Amano et al., 2001). The excessive intracellular Ca^{2+} could induce cell loss in CA3 of SER. The semiology of seizures in SER was different from that of temporal lobe epilepsy. Symptoms of temporal lobe epilepsy did not appear within the lifetime of SER. Further studies are warranted to clarify effects on the inhibitory basket cell in CA1 (in status epileptic models); viz., whether to delay the propagation of epileptic discharge in the SER hippocampus, or attenuate the tonic convulsions in SER.

In conclusion, SER exhibited hippocampal sclerosis-like changes without induction of epileptogenesis. Repetitive tonic seizures and vulnerable CA3 neurons of SER are probably involved in such seizure-related changes in the hippocampus.

4. Experimental procedures

4.1. *Experimental animals*

Mature (age: 8–16 weeks) and immature (age: 4–7 weeks) SER of either sex with convulsive seizures, age-matched Wistar rats, and mature tremor rats (12–25-weeks of age) were used in this study. Wistar and tremor rats were examined at the age of 48–66-weeks, or the age they are deemed to be fully mature. All animals kept in cages in a room maintained at 23±2 °C with 55 ±5% humidity were provided with standard rat chow (MF, Oriental Yeast, Tokyo) and tap water ad libitum.

4.2. *Intracellular recording in hippocampal slices*

After decapitation, the brain was immediately isolated and placed in chilled oxygenated Ca^{2+} free-medium (in mM: 113 NaCl, 3 KCl, 1 NaH_2PO_4, 25 $NaHCO_3$, 5 MgCl, 11 glucose), and hippocampal slices were cut to 400-μm thickness with a microslicer (DTK-1000, Dosaka EM, Japan). After 1- to 2-h incubation in artificial cerebrospinal fluid (ACSF: in mM; 113 NaCl, 3 KCl, 1 NaH_2PO_4, 25 $NaHCO_3$, 5 MgCl, 2 $CaCl_2$, 1 $MgCl_2$, 11 glucose; pH 7.2) at 34 °C, a hippocampal slice was transferred to a recording chamber. ACSF, continuously bubbled with a mixture of 95% O_2 and 5% of CO_2, perfused the slice at 1.5–2 ml/min at room temperature. A bipolar stimulating electrode was then placed in the granule cell layer of the dentate gyrus, and a stimulus (0.1-ms duration, 6–15 V) was delivered to the mossy fiber or Schaffer collateral every 5 s. Intracellular recordings of the hippocampal CA3 pyramidal neurons were performed using a glass microelectrode (electrical resistance; 40–100 M) filled with 3 M KCl. Under the same conditions, a depolarizing pulse (1-nA intensity, 120-ms duration) was applied in the cell through the recording electrode to induce repetitive firing.

The responses were displayed on the digital oscilloscope (VC-10, Nihon Kohden, Japan) after amplification (MEZ-8201, Nihon Kohden), and stored on a personal computer (Macintosh color classic, Apple Inc., USA) using MacLab system (AD Instruments Pty Ltd. Australia) for analysis. The responses were continuously recorded on a thermal array recorder (RTA-1100, Nihon Kohden).

As immature SER do not exhibit abnormal firing in CA3 (Ishihara et al., 1993), intracellular recording was therefore performed in mature animals.

4.3. *Cell count*

Animals were euthanized with 60 mg/kg pentobarbital (i.p.) and perfused transcardially with heparinized saline followed by ice-cold fixative (4% paraformaldehyde in 0.1 M phosphate buffer saline (PBS; pH 7.4). Brains were removed immediately after

perfusion, and postfixed in the same fixative at 4 °C. Anteroposterior coronal paraffin-embedding sections of serially sectioned 4-μm-thick slices were appropriated for investigation. The anteroposterior levels of all sections were uniformly fixed according to stereotactic coordinates of the rat brain atlas of Paxinos and Watson (1996). After hematoxylin–eosin staining, quantification of cell density was performed with a 1-cm^2 microscopic grid (10×10 box) on the coronal sections. The grid for counting was placed on a well-defined area of the cerebral structure of interest, and counting was carried out with a microscopic enlargement of ×200 and ×400 magnifications for each structure.

Cell-counting was performed twice on each side of three adjacent sections for a fixed region by a single observer without any information. The number of cells counted in each brain filed/structure was averaged to minimize potential overestimation errors from double-counting. Neurons touching the inferior and right edge of the grid were not counted. Counts involved only neurons with a cell body larger than 10 μm.

4.4. *Timm's staining*

Brains were removed immediately from euthanized animals previously perfused transcardially with 200 ml of 0.16% Na_2S in 0.1 mol/l PBS (pH 7.3), followed by 400 ml of 3% glutaraldehyde and 0.16% Na_2S in 0.1 mol/l PBS, and then 300 ml of 15% sucrose and 0.16% Na_2S in 0.1 mol/l PB. The isolated brains were immersed for 2 h in the last perfusion solution for cryoprotection, frozen in dry ice, and cut into 20-μm sagittal sections with a microtome. The sections were mounted on slides and developed in a solution containing 75 ml of 20% Arabic gum, 15 ml of a 2% hydroquinone and 3% citric acid mixture, and 1.5 ml of 10% silver nitrate, in the dark for 1 h. The reaction was terminated by immersing in 5% sodium thiosulphate.

4.5. *Immunohistochemistry*

Tissue sections (thickness: 4 μm) were deparaffinized with xylene, and antigen was harvested with the heat-induced epitope retrieval method using citrate buffer solution (pH 6.0). Degrading effects of endogenous peroxidase were inhibited by dipping the slides into a solution containing a mixture of 30% H_2O_2 (10 ml) and 99% methanol (90 ml) for 30 min. Treated slides were rinsed and washed stepwise with PBS (pH 7.5); each step was allocated 3×5-min washings. An indirect method for immunostaining the antibody, or the labeled streptavidin biotin (SAB) method using histofine simplestain (Nichirei Company. Tokyo, Japan), was employed. Immunostaining was performed with a rabbit polyclonal anti-BDNF antibody (1:100, Dako-Cytomation), a rabbit polyclonal anti-caspase-3 antibody (1:50, Gene Tex), and a rabbit polyclonal anti-bax antibody (1/50, Santa Cruz). Primary antibody incubation was performed overnight at 4 °C, followed by 30-min incubation with secondary antibodies (biotinylated secondary antibody, SAB kit; Nichirei Company). The reaction mixture was further incubated for 5–10 min in a mixture of 0.02% diaminobenzidine (DAB tablet; Wako Pure Chemical Industry, Osaka, Japan) and 0.05% H_2O_2 in PBS. All slides were each mounted with a coverslip for storage. Immunohistochemical control sections from two animals underwent similar above-mentioned procedures for all antibodies except for exposure to the primary antibody.

Apoptosis was morphologically assessed by the TUNEL assay using the In-Situ Apoptosis Detection Kit (catalogue MK500; Takara Bio Inc., Ootsu, Japan). The tissue sections (thickness: 4 μm) were deparaffinized with xylene, and stained according to the manufacturer instructions.

4.6. *Densitometric analysis of immunoreactivity*

Images captured by a 3-CCD color video camera (DP 70; Olympus, Tokyo, Japan) mounted on a light microscope (BH 2; Olympus) were relayed to a video monitor and a computer equipped with imaging software (DPC controller, Olympus). The areas of interest selected from the sections and the optical density of each region (demarcated according to the rat brain atlas) were measured by a blind reader. Images of all areas of interest were captured at ×40- or ×100-magnification. The color images were transformed to black and white images and analyzed accordingly (Image J software; (NIH, USA). Immunoreactivity was expressed as optical density (OD). Standard transfer curves of the gray level produced by filters of known OD (Kodak, New York, USA) were used to calibrate the measurement system. The mean value of each area per rat was calculated using the values from three sections. The corpus callosum, which does not have synaptic terminals, was selected for background calculation because it was included in slices examined in this study and the hyperexpression of BDNF has not been reported as yet. Each value was obtained from the difference between the value of region-of-interest and that of corpus callosum.

4.7. *Statistical analysis*

The values obtained in the SER were compared with those of tremor rat, and normal Wistar rats. Group comparisons were determined initially by analysis of variance (ANOVA) for independent groups followed by the Scheffe's test.

REFERENCES

Amano, T., Amano, H., Matsubayashi, H., Ishihara, K., Serikawa, T., Sasa, M., 2001. Enhanced Ca(2+) influx with mossy fiber stimulation in hippocampal CA3 neurons of spontaneously epileptic rats. Brain Res. 910, 199–203.

Avoli, M., D'Antuono, M., Louvel, J., Köhling, R., Biagini, G., Pumain, R., D'Arcangelo, G., Tancredi, V., 2002. Network and pharmacological mechanisms leading to epileptiform synchronization in the limbic system in vitro. Prog. Neurobiol. 68, 167–207.

Bengzon, J., Mohapel, P., Ekdahl, C.T., Lindvall, O., 2002. Neuronal apoptosis after brief and prolonged seizures. Prog. Brain Res. 135, 111–119.

Binder, D.K., 2007. Neurotrophins in the dentate gyrus. Prog. Brain Res. 163, 371–397.

Bote, R.P., Blázquez-Llorca, L., Fernández-Gil, M.A., Alonso-Nanclares, L., Muñoz, A., De Felipe, J., 2008. Hippocampal sclerosis: histopathology substrate and magnetic resonance imaging. Semin. Ultrasound CT MR 29, 2–14.

Cavazos, J.E., Das, I., Sutula, T.P., 1994. Neuronal loss induced in limbic pathways by kindling: evidence for induction of hippocampal sclerosis by repeated brief seizures. J. Neurosci. 14, 3106–3121.

Danober, L., Deransart, C., Depaulis, A., Vergnes, M., Marescaux, C., 1998. Pathophysiological mechanisms of genetic absence epilepsy in the rat. Prog. Neurobiol. 55, 27–57.

Ebert, U., Brandt, C., Löscher, W., 2002. Delayed sclerosis, neuroprotection, and limbic epileptogenesis after status epilepticus in the rat. Epilepsia 43 (supple), 86–95.

Gohma, H., Kuramoto, T., Matalon, R., Surendran, S., Tyring, S., Kitada, K., Sasa, M., Serikawa, T., 2007. Absence-like and tonic seizures in aspartoacylase/attractin double-mutant mice Exp. Anim. 56, 161–165.

Gorter, J.A., Gonçalves, Pereira, P.M., van Vliet, E.A., Aronica, E., Lopes, da Silva, F.H., Lucassen, P.J., 2003. Neuronal cell death in a rat model for mesial temporal lobe epilepsy is induced by the initial status epilepticus and not by later repeated spontaneous seizures. Epilepsia 44, 647–658.

Gurbanova, A.A., Aker, R.G., Sirvanci, S., Demiralp, T., Onat, F.Y., 2008. Intra-amygdaloid injection of kainic acid in rats with genetic absence epilepsy: the relationship of typical absence epilepsy and temporal lobe epilepsy. J. Neurosci. 28, 7828–7836.

Hanaya, R., Sasa, M., Ujihara, H., Fujita, Y., Amano, T., Matsubayashi, M., Serikawa, T., Uozumi, T., 1995. Effect of antiepileptic drugs on absence-like seizures in the tremor rat. Epilepsia 36, 938–942.

Hanaya, R., Sasa, M., Ujihara, H., Ishihara, K., Serikawa, T., Iida, K., Akimitsu, T., Arita, K., Kurisu, K., 1998. Suppression by topiramate of epileptiform burst discharges in hippocampal CA3 neurons of spontaneously epileptic rat in vitro. Brain Res. 789, 274–282.

Hanaya, R., Koning, E., Ferrandon, A., Nehlig, A., 2008. The role of the inherited genetic background on the consequences of lithium-pilocarpine status epilepticus: study in Genetic Absence Epilepsy Rats from Strasbourg and Wistar audiogenic rats. Neurobiol. Dis. 31, 451–458.

Hughes, P.E., Alexi, T., Walton, M., Williams, C.E., Dragunow, M., Clark, R.G., Gluckman, P.D., 1999. Activity and injury-dependent expression of inducible transcription factors, growth factors and apoptosis-related genes within the central nervous system. Prog. Neurobiol. 57, 421–450.

Ishihara, K., Sasa, M., Momiyama, T., Ujihara, H., Nakamura, J., Serikawa, T., Yamada, J., Takaori, S., 1993. Abnormal excitability of hippocampal CA3 pyramidal neurons of spontaneously epileptic rats (SER), a double mutant. Exp. Neurol. 119, 287–290.

Kandel, A., Bragin, A., Carpi, D., Buzsáki, G., 1996. Lack of hippocampal involvement in a rat model of petit mal epilepsy. Epilepsy Res. 23, 123–127.

Kitada, K., Akimitsu, T., Shigematsu, Y., Kondo, A., Maihara, T., Yokoi, N., Kuramoto, T., Sasa, M., Serikawa, T., 2000. Accumulation of N-acetyl-L-aspartate in the brain of the tremor rat, a mutant exhibiting absence-like seizure and spongiform degeneration in the central nervous system J. Nerochem. 74, 2512–2519.

Koyama, R., Yamada, M.K., Fujisawa, S., Katoh-Semba, R., Matsuki, N., Ikegaya, Y., 2004. Brain-derived neurotrophic factor induces hyperexcitable reentrant circuits in the dentate gyrus. J. Neurosci. 24, 7215–7224.

Limbrick Jr., D.D., Sombati, S., DeLorenzo, R.J., 2003. Calcium influx constitutes the ionic basis for the maintenance of glutamate-induced extended neuronal depolarization associated with hippocampal neuronal death. Cell Calcium 33, 69–81.

Luhmann, H.J., Mittmann, T., van Luijtelaar, G., Heinemann, U., 1995. Impairment of intracortical GABAergic inhibition in a rat model of absence epilepsy. Epilepsy Res. 22, 43–51.

Mathern, G.W., Babb, T.L., Leite, J.P., Pretorius, K., Yeoman, K.M., Kuhlman, P.A., 1996. The pathogenic and progressive features of chronic human hippocampal epilepsy. Epilepsy Res. 26, 151–161.

Mello, L.E., Cavalheiro, E.A., Tan, A.M., Kupfer, W.R., Pretorius, J.K., Babb, T.L., Finch, D.M., 1993. Circuit mechanisms of seizures in the pilocarpine model of chronic epilepsy: cell loss and mossy fiber sprouting. Epilepsia 34, 985–995.

Paxinos, G., Watson, C., 1996. The Rat Brain in Stereotaxic Coordinates, 3rd ed. Academic Press, San Diego.

Qiao, X., Noebels, J.L., 1993. Developmental analysis of hippocampal mossy fiber outgrowth in a mutant mouse with inherited spike-wave seizures. J. Neurosci. 13, 4622–4635.

Rhem, S., Mehraein, P., Anzil, A.P., Deerberg, F., 1982. A new rat mutant with detective overhairs and spongy degeneration of the central nervous system: clinical pathological studies. Lab. Anim. Sci. 32, 70–73.

Saji, H., Iida, Y., Takahashi, M., Sasa, M., Serikawa, T., Yamada, J., Yokoyama, A., 1993. Local cerebral glucose utilization in the interictal state of the spontaneously epileptic rat (SER). Brain Res. 601, 76–79.

Sasa, M., Ohno, Y., Ujihara, H., Fujita, Y., Yoshimura, M., Takaori, S., Serikawa, T., Yamada, J., 1988. Effects of antiepileptic drugs on absence-like and tonic seizures in the spontaneously epileptic rat, a double mutant rat. Epilepsia 29, 505–513.

Scharfman, H.E., 1997. Hyperexcitability in combined entorhinal/hippocampal slices of adult rat after exposure to brain-derived neurotrophic factor. J. Neurophysiol. 78, 1082–1095.

Scharfman, H.E., Goodman, J.H., Du, F., Schwarcz, R., 1998. Chronic changes in synaptic responses of entorhinal and hippocampal neurons after amino-oxyacetic acid (AOAA)-induced entorhinal cortical neuron loss. J. Neurophysiol. 80, 3031–3046.

Schmidt-Kastner, R., Wetmore, C., Olson, L., 1996. Comparative study of brain-derived neurotrophic factor messenger RNA and protein at the cellular level suggests multiple roles in hippocampus, striatum and cortex. Neuroscience 74, 161–183.

Serikawa, T., Yamada, J., 1986. Epileptic seizures in rats homozygous for two mutations, zitter and tremor. J. Hered. 77, 441–444.

Serikawa, T., Ohno, Y., Sasa, M., Yamada, J., Takaori, S., 1987. A new model of petit mal epilepsy: spontaneous spike and wave discharges in tremor rats. Lab. Anim. 21, 68–71.

Sirvanci, S., Meshul, C.K., Onat, F., San, T., 2003. Immunocytochemical analysis of glutamate and GABA in hippocampus of genetic absence epilepsy rats (GAERS). Brain Res. 988, 180–188.

Sloviter, R.S., 1991. Permanently altered hippocampal structure, excitability, and inhibition after experimental status epilepticus in the rat: the dormant basket cell hypothesis and its possible relevance to temporal lobe epilepsy Hippocampus 1, 41–66.

Sloviter, R.S., 2008. Hippocampal epileptogenesis in animal models of mesial temporal lobe epilepsy with hippocampal sclerosis: the importance of the "latent period" and other concepts. Epilepsia 49 (Suppl), 85–92.

Tolmacheva, E.A., van Luijtelaar, G., Chepurnov, S.A., Kaminskij, Y., Mares, P., 2004. Cortical and limbic excitability in rats with absence epilepsy. Epilepsy Res. 62, 189–198.

Uysal, H., Cevik, I.U., Soylemezoglu, F., Elibol, B., Ozdemir, Y.G., Evrenkaya, T., Saygi, S., Dalkara, T., 2003. Is the cell death in mesial temporal sclerosis apoptotic? Epilepsia 44, 778–784.

Weise, J., Engelhorn, T., Dörfler, A., Aker, S., Bähr, M., Hufnagel, A., 2005. Expression time course and spatial distribution of activated caspase-3 after experimental status epilepticus: contribution of delayed neuronal cell death to seizure-induced neuronal injury. Neurobiol. Dis. 18, 582–590.

Wozny, C., Gabriel, S., Jandova, K., Schulze, K., Heinemann, U., Behr, J., 2005. Entorhinal cortex entrains epileptiform activity in CA1 in pilocarpine-treated rats. Neurobiol. Dis. 19, 451–460.

Xu, S., Pang, Q., Liu, Y., Shang, W., Zhai, G., Ge, M., 2007. Neuronal apoptosis in the resected sclerotic hippocampus in patients with mesial temporal lobe epilepsy. J. Clin. Neurosci. 14, 835–840.

Yamada, J., Serikawa, T., Ishiko, J., Inui, T., Takada, H., Kawai, Y., Okaniwa, A., 1985. Rats with congenital tremor and curled whisker and hair. Exp. Anim. 34, 183–188.

Yan, H.D., Ishihara, K., Hanaya, R., Kurisu, K., Serikawa, T., Sasa, M., 2007. Voltage-dependent calcium channel abnormalities in hippocampal CA3 neurons of spontaneously epileptic rats. Epilepsia 48, 758–764.

NOTE *Laboratory Animal Science*

Identification of the Rat *Rex* Mutation as a 7-bp Deletion at Splicing Acceptor Site of the *Krt71* Gene

Takashi KURAMOTO[1)]*, Ryuji HIRANO[2)], Mitsuru KUWAMURA[2)] and Tadao SERIKAWA[1)]

[1)]*Institute of Laboratory Animals, Graduate School of Medicine, Kyoto University, Yoshidakonoe-cho, Sakyo-ku, Kyoto 606–8501 and* [2)]*Laboratory of Veterinary Pathology, Osaka Prefecture University, Rinku Orai-Kita, Izumisano, Osaka 598–8531, Japan*

(Received 9 December 2009/Accepted 9 February 2010/Published online in J-STAGE 23 February 2010)

ABSTRACT. The rat autosomal dominant Rex (*Re*) mutation on chromosome 7 causes curly hair in *Re*/+ and hair loss in *Re/Re* rats. Histopathologically, the *Re*/+ rat showed dilatation of the hair follicle and hairs with irregularly-coated cuticles, and the *Re/Re* rat showed more severe effects. We identified *Re* as a 7-bp deletion at the splicing acceptor site of intron 1 of the keratin 71 (*Krt71*) gene, which is located within the *Re* critical chromosomal region and plays an important role in hair formation. The deletion provoked a 6-amino acid in-frame deletion (p.Val149_Gln154del) in the α-helical rod domain of KRT71 protein. Identification of the *Re* mutation ($Krt71^{Re}$) enables us to further understand the biological function of KRT71.

KEY WORDS: Krt71, mutation, rat, wavy hair.

J. Vet. Med. Sci. 72(7): 909–912, 2010

The laboratory rat (*Rattus norvegicus*) has been widely used as an animal model of human diseases, because its size is suitable for manipulation [1, 12]. The rat model system is also used for understanding gene function. Thus, characterization of rat mutations leads to the establishment of a disease model as well as the enhancement of gene function analyses. Recently, we introduced 9 fancy-derived mutations into our laboratory. Among them, autosomal dominant Rex (*Re*) mutation caused typical rexoid or curly coat hair and vibrissae in *Re*/+ rats [7]. Origin of the *Re* is unknown, but it was imported from U.K. to a fancy rat breeder in California of U.S.A., and then given to the breeder in Kansas City, from which rats carrying *Re* mutation were introduced to our laboratory in 2005 [7]. The *Re* mutation is carried in a fancy-derived inbred strain, KFRS5A/Kyo, and has been mapped to the distal part of chromosome (Chr) 7 [7]. In this study, we characterized the *Re* mutation morphologically and identified the *Re* mutation.

KFRS5A/Kyo strains were obtained from the National BioResource Project – Rat (NBRP-Rat) [12]. For histopathology, dorsal skins were collected from *Re/Re*, *Re*/+, and wild-type (+/+) rats, fixed in 10% buffered formalin, and embedded in paraffin. Paraffin sections (4 μm) were stained with hematoxylin and eosin (HE). For scanning electron microscopy (SEM), dorsal hairs were collected and covered with ionized gold and observed under a scanning electron microscopy (JSM6510LV, JEOL, Tokyo, Japan). For mutation detection, RT-PCR products of candidate gene were sequenced. We isolated mRNA from the dorsal skin of 5-week-old *Re/Re* rats and performed RT-PCR with 4 sets of primers, rK6irs1-1&2; CTACAGCCAGTACAACCTTCG and GGCGAACTTGTTGTTCAGTG, rK6irs1–3&4; CCACCAGGTCACAGTCAATG and TGTCCAGGTCCAGGTTCCTA, rK6irs1–5&6; GAACTGCAGGCTAAGGTGGA and CCAGACATCCTGCACTCCTC, rK6irs1–7&8; AGGATGCTGCGTGAATACCA and GGCTGGACCTGAGCTGAA. PCR products amplified by these primer sets overlapped and covered the entire *Krt71* coding sequence (CDS). All experimental procedures in this study were approved by the Animal Research Committee, Graduate School of Medicine, Kyoto University.

In *Re/Re*, rats had a more severe effects in the coat and vibrissae phenotype than in *Re*/+ rats. The body hair of *Re/Re* rats was completely lost by 5 weeks of age (Fig. 1A), and sparse coat hair appeared in adulthood. Histopathological examination of dorsal skin samples revealed dilatation of the hair follicle in *Re/Re* rats. The dilated cyst was lined by a flattened squamous epithelium with a granular cell layer. The cyst contained attenuated hair shafts and many keratin debris. In the *Re*/+ rat, mildly dilated hair follicles were seen compared to those of wild-type rat (Fig. 1B). SEM revealed that dorsal hairs of *Re/Re* rats were frequently reduced in diameter compared with the wild type. The hair cuticles of *Re/Re* were coated irregularly, whereas cuticles of the wild-type were arranged tidily (Fig. 1C).

The *Re* locus encompassed about a 10-Mb region (132.6 Mb to 142.4 Mb) and contained the type II keratin gene cluster where at least 24 keratin genes are assigned [5, 7]. Among them, keratin 71 (*Krt71*) (previously, *K6irs1* or *Krt2–6g*) is a good candidate because *Krt71*-mutant mice display wavy pelage and curly vibrissae, which are inherited in an autosomal dominant manner [6, 11]. This prompted us to investigate nucleotide alterations in the *Krt71* gene of KFRS5A/Kyo rats. In *Re/Re* rats, a 18-bp nucleotide deletion was found at the exon 1-exon 2 boundary, defined by the 444th and 445th nucleotide of the *Krt71* CDS (Fig. 2A). Because the deleted 18-bp nucleotide encoded 6 in-frame

* CORRESPONDENCE TO: KURAMOTO, T., Institute of Laboratory Animals, Graduate School of Medicine, Kyoto University, Yoshida-konoe-cho, Sakyo-ku, Kyoto 606–8501, Japan.
e-mail: tkuramot@anim.med.kyoto-u.ac.jp

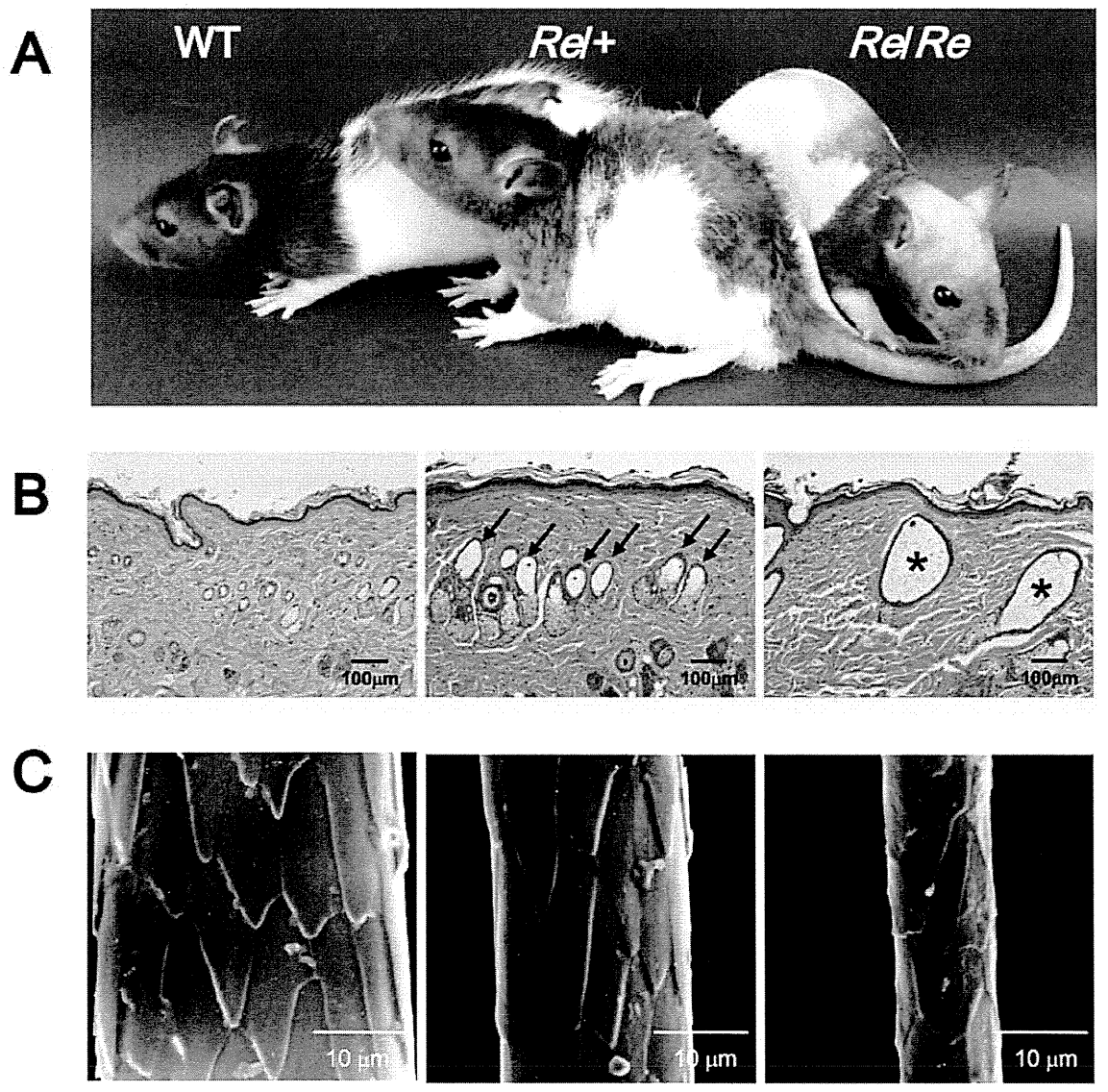

Fig. 1. External phenotypes and histopathology of *Re/+* and *Re/Re* rats. A, External appearance of body hair of wild-type (left), *Re/+* heterozygous (center), and *Re/Re* homozygous (right) rats. B, Histopathology of dorsal skin from wild-type (left), *Re/+* (center), and *Re/Re* (right) rats. Hair follicles in the *Re/Re* rat were markedly dilated and contained hair shafts and keratin debris and were indicated by asterisks. Mild dilatation of the hair follicle was noted in the *Re/+* rat and indicated by arrows. HE staining. C, SEM images of the hairs of wild-type (left), *Re/+* (center) and *Re/Re* (right) rats. The hair of the *Re/Re* rat was reduced in diameter and hair cuticles were irregularly arranged.

amino acids (VRFLEQ, 149th to 154th residues), the *Krt71* transcript from the *Re* allele was predicted to encode a protein 6 amino acids smaller than that of the wild type (Fig. 2A). These findings indicated that the *Re* rat harbored either a mutation influencing transcriptional splicing in intron 1 or a deletion of a part of exon 2.

To identify genomic nucleotide alteration of the *Krt71* gene in the KFRS5A/Kyo rat, we amplified the exon 1-intron 1 boundary and the intron 1-exon 2 boundary, and determined their sequences. A 7-bp deletion, which comprised the 6-bp consensus acceptor site (TTCCAG) and the first nucleotide of exon 2 (G), was found at the intron 1-exon 2 boundary (Fig. 2B, C). Comparison of cDNA with genomic sequences of the *Krt71* exon 2 suggested that the AG di-nucleotide sequence 18-bp downstream of the original splicing acceptor site might serve as an alternative splicing acceptor site in the *Re* mutant allele (Fig. 2B).

KRT71 belongs to a family of type II keratins that are specifically expressed in the inner root sheath (IRS) of hair follicles [2, 9]. Rat KRT71 is a 524-amino acid protein and consists of a head (130-amino acid), α-helical rod (310-amino acid), and tail (84-amino acid) (Fig. 2D). The α-heli-

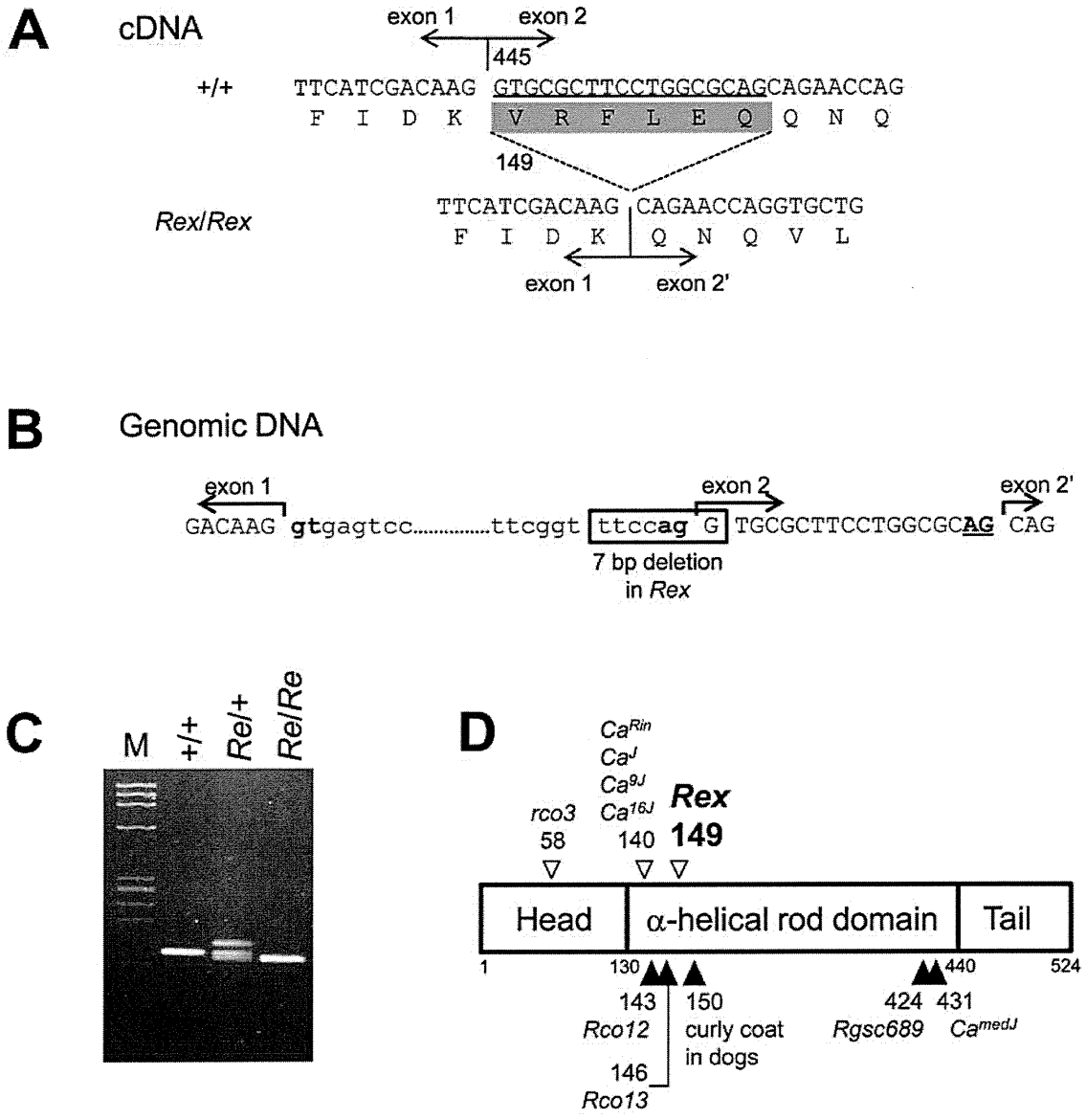

Fig. 2. Identification of the *Re* mutation. A, Nucleotide sequences of the exon 1-exon 2 boundary of *Krt71* cDNA of wild-type (upper) and *Re/Re* (lower) rats. The deduced amino acid sequences are shown below the cDNA sequences. In *Re/Re* cDNA, 18-bp nucleotide (underlined in the wild type) was lost, so the 6 in-frame residues (grey rectangle) were lost in KRT71. B, Genomic DNA sequences of the exon 1-intron 1 boundary and the intron 1-exon 2 boundary of the *Krt71* gene. In the *Re* allele, 7-bp deletion (boxed) at the splicing acceptor site was found. The AG sequence 18-bp downstream of the original splicing acceptor site (underlined) was utilized as an alternative acceptor site in the *Re/Re* rats. C, Detection of the *Re* mutation by PCR. M: molecular marker, ϕX174-*Hae*III digest. Primer sequences (rKrt71-Rex-F&R) are as follows: TCAAGTATCT-GTGGGGCTCA and CCAGGTTGTTCTTGCAGTTG. Note that PCR product from the *Re/Re* rat is 7-bp smaller than that from the +/+ rat (135 bp). In the *Re/+* rat, both mutant and wild-type bands were observed. The extra band (largest) in *Re/+* is generated by interaction of PCR products derived from the wild-type and *Re* alleles. D, Schematic representation of known mutations in the *Krt71* gene. The keratin protein consists of three domains, a head domain, a tail domain, and the helix-forming α-helical rod domain. Open arrowheads indicate the deletion mutation sites that include several *Caracul* alleles (N140 del in $Ca^{Rin, J, 9J, 16J}$) and the *rco3* allele (10-bp deletion inducing complete lack of the α-helical rod domain). Filled arrowheads indicate the missense mutation sites in mouse *Rco12* (A143→D), *Rco13* (I146→F), *Rgsc689* (L424 →W), and Ca^{medJ} (A431→D) [6]. A SNP associated with curly coat in domestic dogs (R151→W) is also indicated by filled arrowhead. The dog R151 residue corresponds to the R150 residue in the rat KRT71 ortholog.

cal rod domain of KRT71 plays an important role in forming heteropolymers of a specific type I and type II cytokeratin through interactions of these domains [4]. Mutations located in the α-helical rod domain affected morphology of the IRS, resulting in curly body hair. For example, mouse mutations, such as Ca^{Rin}, Ca^{J}, Ca^{9J}, and Ca^{16J}, induce 1-amino acid deletion at the position of 140-amino acid and result in curly body hair [6]. Missense mutations at positions 143 and 146, such as *Rco12* and *Rco13*, also result in curly body hair [11]. A single nucleotide polymorphism (SNP) causing a non-synonymous alteration (Arg151→Trp) has been recently identified to be associated with curly hair in dogs [3]. Deletion at the splicing acceptor site of *Krt71* in KFRS5A/Kyo was deduced to induce the 6-amino acid deletion in the α-helical rod of KRT71. Thus, we concluded that the *Re* mutation was a 7-bp deletion at the splicing acceptor site of *Krt71*. It is likely that the mutated KRT71 would interact with its specific counterpart of type I keratin [13], which might explain the dominant wavy coat phenotype.

In the current study, we demonstrated that phenotypes of *Re/Re* rats were severer than *Re*/+ rats. In mice, phenotypes of homozygotes for *Krt71* mutations have not been described in the dominant-type mutations, while phenotype of a recessive mutant mouse, $Krt71^{rco3}/Krt71^{rco3}$, have been characterized as patchy alopecia [10]. Although *Re* mutation induced only 6 amino acids deletion in KRT71, it seems *Re/Re* phenotype would be severer than *rco3/rco3* phenotype. The IRS-specific type II keratins form heterodimers with the IRS-specific type I keratins and their expressions are overlapped [8, 9, 13]. Among four known IRS-specific type II keratins, KRT71 is dominantly expressed in the IRS [9]. Thus, it is speculated that expression of *Re*-type KRT71 could form heterodimers with its type I keratin counterpart and malformed hairs would be produced. Meanwhile, in *rco3/rco3* mice, severely reduced expression of KRT71 might be partially compensated by other IRS-specific type II keratins.

Our current study demonstrates the importance of the α-helical rod domain of KRT71 in hair formation in rats as well as mice and dogs. Comparison of *Krt71* mutations in various species may allow us to find association of pelage phenotype with type of mutations, which leads better understanding of KRT71 functions. Moreover, this study suggests a subset of curly hair and atrichia phenotype might be associated with *Krt71* mutation in human as well as domestic animals.

This work was supported in part by Grants-in-aid for Scientific Research from the Japan Society for the Promotion of Science (21300153 to TK) and a Grant-in-aid for Cancer Research from the Ministry of Health, Labour and Welfare. We are grateful to M. Yokoe for her excellent technical assistance and the National BioResource Project - Rat for providing the KFRS5A/Kyo strain (NBPR#0573).

REFERENCES

1. Aitman, T. J., Critser, J. K., Cuppen, E., Dominiczak, A., Fernandez-Suarez, X. M., Flint, J., Gauguier, D., Geurts, A. M., Gould, M., Harris, P. C., Holmdahl, R., Hubner, N., Izsvak, Z., Jacob, H. J., Kuramoto, T., Kwitek, A. E., Marrone, A., Mashimo, T., Moreno, C., Mullins, J., Mullins, L., Olsson, T., Pravenec, M., Riley, L., Saar, K., Serikawa, T., Shull, J. D., Szpirer, C., Twigger, S. N., Voigt, B. and Worley, K. 2008. Progress and prospects in rat genetics: a community view. *Nat. Genet.* **40**: 516–522.
2. Aoki, N., Sawada, S., Rogers, M. A., Schweizer, J., Shimomura, Y., Tsujimoto, T., Ito, K. and Ito, M. 2001. A novel type II cytokeratin, mK6irs, is expressed in the Huxley and Henle layers of the mouse inner root sheath. *J. Invest. Dermatol.* **116**: 359–365.
3. Cadieu, E., Neff, M. W., Quignon, P., Walsh, K., Chase, K., Parker, H. G., Vonholdt, B. M., Rhue, A., Boyko, A., Byers, A., Wong, A., Mosher, D. S., Elkahloun, A. G., Spady, T. C., Andre, C., Lark, K. G., Cargill, M., Bustamante, C. D., Wayne, R. K. and Ostrander, E. A. 2009. Coat variation in the domestic dog is governed by variants in three genes. *Science* **326**: 150–153.
4. Hatzfeld, M. and Weber, K. 1990. The coiled coil of *in vitro* assembled keratin filaments is a heterodimer of type I and II keratins: use of site-specific mutagenesis and recombinant protein expression. *J. Cell Biol.* **110**: 1199–1210.
5. Hesse, M., Zimek, A., Weber, K. and Magin, T. M. 2004. Comprehensive analysis of keratin gene clusters in humans and rodents. *Eur. J. Cell Biol.* **83**: 19–26.
6. Kikkawa, Y., Oyama, A., Ishii, R., Miura, I., Amano, T., Ishii, Y., Yoshikawa, Y., Masuya, H., Wakana, S., Shiroishi, T., Taya, C. and Yonekawa, H. 2003. A small deletion hotspot in the type II keratin gene *mK6irs1/Krt2–6g* on mouse chromosome 15, a candidate for causing the wavy hair of the caracul (*Ca*) mutation. *Genetics* **165**: 721–733.
7. Kuramoto, T., Yokoe, M., Yamasaki, K., Kawaguchi, T., Kumafuji, K. and Serikawa, T. 2010. Genetic analysis of fancy rat derived mutations. *Exp. Anim.* **59**: 147–155.
8. Langbein, L., Rogers, M. A., Praetzel-Wunder, S., Helmke, B., Schirmacher, P. and Schweizer, J. 2006. K25 (k25irs1), k26 (k25irs2), k27 (k25irs3), and k28 (k25irs4) represent the type I inner root sheath keratins of the human hair follicle. *J. Invest. Dermatol.* **126**: 2377–2386.
9. Langbein, L., Rogers, M. A., Praetzel, S., Winter, H. and Schweizer, J. 2003. K6irs1, K6irs2, K6irs3, and K6irs4 represent the inner-root-sheath-specific type II epithelial keratins of the human hair follicle. *J. Invest. Dermatol.* **120**: 512–522.
10. Peters, T., Sedlmeier, R., Bussow, H., Runkel, F., Luers, G. H., Korthaus, D., Fuchs, H., Hrabe de Angelis, M., Stumm, G., Russ, A. P., Porter, R. M., Augustin, M. and Franz, T. 2003. Alopecia in a novel mouse model RCO3 is caused by mK6irs1 deficiency. *J. Invest. Dermatol.* **121**: 674–680.
11. Runkel, F., Klaften, M., Koch, K., Bohnert, V., Bussow, H., Fuchs, H., Franz, T. and Hrabe de Angelis, M. 2006. Morphologic and molecular characterization of two novel *Krt71 (Krt2–6g)* mutations: $Krt71^{rco12}$ and $Krt71^{rco13}$. *Mamm. Genome* **17**: 1172–1182.
12. Serikawa, T., Mashimo, T., Takizawa, A., Okajima, R., Maedomari, N., Kumafuji, K., Takami, F., Neoda, Y., Otsuki, M., Nakanishi, S., Yamasaki, K., Voigt, B. and Kuramoto, T. 2009. National BioResource Project - Rat and related activities. *Exp. Anim.* **58**: 333–341.
13. Tanaka, S., Miura, I., Yoshiki, A., Kato, Y., Yokoyama, H., Shinogi, A., Masuya, H., Wakana, S., Tamura, M. and Shiroishi, T. 2007. Mutations in the helix termination motif of mouse type I IRS keratin genes impair the assembly of keratin intermediate filament. *Genomics* **90**: 703–711.

Epilepsy Research (2010) **89**, 360–364

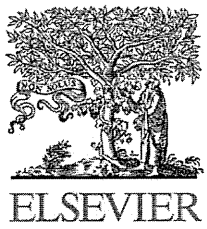

journal homepage: www.elsevier.com/locate/epilepsyres

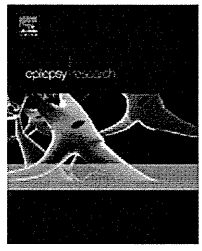

SHORT COMMUNICATION

Antiepileptogenic and anticonvulsive actions of levetiracetam in a pentylenetetrazole kindling model

Yukihiro Ohno[a,*], Shizuka Ishihara[a], Ryo Terada[a], Tadao Serikawa[b], Masashi Sasa[c]

[a] *Laboratory of Pharmacology, Osaka University of Pharmaceutical Sciences, 4-20-1 Nasahara, Takatsuki, Osaka 569-1094, Japan*
[b] *Institute of Laboratory Animals, Graduate School of Medicine, Kyoto University, Sakyo-ku, Kyoto 606-8501, Japan*
[c] *Nagisa Clinic, Hirakata, Osaka 573-1183, Japan*

Received 18 December 2009; received in revised form 6 January 2010; accepted 16 January 2010
Available online 6 February 2010

KEYWORDS
Levetiracetam;
Antiepileptic drugs;
Kindling;
Epileptogenesis;
Pentylenetetrazole

Summary Levetiracetam (LEV) is a unique antiepileptic drug that preferentially interacts with synaptic vesicle protein 2A (SV2A). To evaluate the antiepileptogenic action of LEV, we studied its effects on the development and acquisition of pentylenetetrazole (PTZ) kindling and compared them to those of sodium valproate (VPA). Anticonvulsive actions of LEV in PTZ-kindled animals were also determined. LEV did not affect PTZ seizures in naïve animals even at high doses (≈300 mg/kg, i.p.). However, combined treatment of LEV (30 and 100 mg/kg, i.p.) with PTZ significantly suppressed the development and acquisition of PTZ kindling. In addition, LEV at relatively low doses (3–30 mg/kg, i.p.) inhibited PTZ-evoked seizures in fully kindled animals. In contrast to LEV, VPA at sub-anticonvulsive doses (30 and 100 mg/kg, i.p.) failed to prevent the development of PTZ kindling and its anticonvulsive potency was similar in PTZ-kindled and naïve mice. The present study shows that LEV contrasts VPA by preventing the development of PTZ kindling and inhibiting seizures selectively in kindled animals.

Introduction

Levetiracetam (LEV) is a unique antiepileptic drug (AED) which preferentially interacts with synaptic vesicle protein 2A (SV2A) without affecting activities of neurotransmitter receptors or ion channels (Lynch et al., 2004; Sasa, 2006; Kaminski et al., 2008). Unlike conventional AEDs, LEV is not active in the classical convulsion tests (i.e., maximal electroshock- and maximal pentylenetetrazole (PTZ)-evoked seizures) (Löscher and Hönack, 1993; Klitgaard et al., 1998; Bastlund et al., 2005), but it inhibits seizures in various animal models including kindled animals (e.g., corneal- and amygdala kindling) (Löscher and Hönack, 1993; Klitgaard et al., 1998; Löscher et al., 1998) and genetically defined animal models of epilepsy (Gower et al., 1995; Bouwman and van Rijn, 2004; Yan et al., 2005; Jiqun et al., 2005). In addition, previous studies demonstrated that LEV can inhibit the development of amygdala kindling in rats, suggesting that LEV has antiepileptogenic activi-

* Corresponding author. Tel.: +81 72 690 1052; fax: +81 72 690 1053.
E-mail address: yohno@gly.oups.ac.jp (Y. Ohno).

0920-1211/$ – see front matter © 2010 Elsevier B.V. All rights reserved.
doi:10.1016/j.eplepsyres.2010.01.011

Table 1 Anticonvulsive effects of LEV and VPA in PTZ-kindled and naïve mice.

	Naïve animals				PTZ-kindled animals			
	Test dose (mg/kg, i.p.)	Inhibition of PTZ seizures		ED_{50} (mg/kg, i.p.)	Test dose (mg/kg, i.p.)	Inhibition of PTZ seizures		ED_{50} (mg/kg, i.p.)
		No. of animals	% Inhibition			No. of animals	% Inhibition	
LEV	30	0/6*	0	>300	3	0/16	0	27.3
	100	0/6	0		10	6/15	40	(18.7–58.7)
	300	0/6	0		30	8/16	50	
VPA	100	1/6	17	229	100	2/8	25	227
	200	1/6	17	(151.5–300.4)	300	5/8	62	(46.6–389.3)
	300	5/6	83		600	7/7	100	
	400	6/6	100					

Seizures were evoked by 70 mg/kg (i.p.) PTZ in naïve mice and by 40 mg/kg (i.p.) PTZ in PTZ-kindled mice. VPAs in parentheses under the ED_{50} values indicate 95% confidence limits.
* Number of animals in which PTZ-evoked seizures were inhibited/total number of animals examined.

ties (Löscher et al., 1998; Husum et al., 2004; Gu et al., 2004). Nonetheless, a recent study by Matveeva et al. (2008) showed that LEV retarded the development of amygdala kindling, but could not prevent kindling acquisition. Studies using animals with spontaneous recurrent seizures after status epilepticus also demonstrated the lack of effectiveness of LEV against the epileptogenesis (Brandt et al., 2007). Thus, the antiepileptogenic potential of LEV is still unclear and remains to be verified using different animal models.

In order to address this question further, we studied the effects of LEV on the development and acquisition of PTZ-induced kindling in mice, and compared them with those of the typical AED sodium valproate (VPA).

Methods

Male ddY mice (Japan SLC, Shizuoka, Japan) weighing 20–25 g were used. Animals were housed in air-conditioned rooms under a 12-h light/dark cycle (light on: 7:00 a.m.) and allowed *ad libitum* access to food and water. The housing conditions of the mice and animal care methods complied with NIH guide for the care and use of laboratory animals. The experimental protocols of this study were approved by the Experimental Animal Research Committee at Osaka University of Pharmaceutical Sciences.

In order to set the test doses of LEV and VPA for PTZ kindling, we first determined their anticonvulsive actions against maximal PTZ seizures using naïve mice (Bastlund et al., 2005). Namely, animals were first given with different doses of LEV or VPA, and 30 min later, PTZ (70 mg/kg, i.p.) was injected. The incidence and severity of seizures were evaluated over 15 min immediately after the PTZ injection, using a 4-point ranked scale (0: none; 1: occasional head twitches; 2: myoclonic jerk or partial clonic seizure of forepaws and/or upper body trunk; 3: generalized clonic seizures). The observers were kept blind to the drug treatment, and the incidence of PTZ-induced seizures was judged as positive when the animal showed a score 2 or more.

PTZ kindling was induced as published previously (Ohno et al., 2009). Briefly, animals were given a sub-convulsive dose of PTZ (40 mg/kg, i.p.) every weekday for 12 days. For the evaluation of antiepileptogenic activity, LEV or VPA at the doses which negligibly affect PTZ seizures by themselves was repeatedly administered to the animals 30 min before PTZ injection for 12 days. The incidence and severity of the PTZ-evoked seizures were evaluated over 15 min immediately after the PTZ injection in the same manner as described above.

We also determined the anticonvulsive actions of LEV and VPA in PTZ-kindled animals. The mice were treated with PTZ (40 mg/kg, i.p.) every weekday for 15 days, and only PTZ-kindled mice (exhibiting seizures at least 3 successive days) were subjected to the anticonvulsive test for LEV and VPA. On the day of experiments, animals were first given with different doses of LEV, VPA or the vehicle, and 30 min later, PTZ (40 mg/kg, i.p.) was injected. Incidence and severity of PTZ-evoked seizures were evaluated over 15 min immediately after the PTZ injection in the same manner as described previously.

PTZ hydrochloride and VPA hydrochloride were purchased from Sigma–Aldrich. LEV was a gift from UCB Japan (Tokyo, Japan). All drugs were dissolved in saline and injected at a volume of 5 ml/kg.

Results

In naïve animals, LEV did not affect PTZ seizures even at high doses up to 300 mg/kg (i.p.) while VPA inhibited the seizures with an ED_{50} value of 229 mg/kg (i.p.) (Table 1). We therefore set the test doses of LEV and VPA at 30 and 100 mg/kg

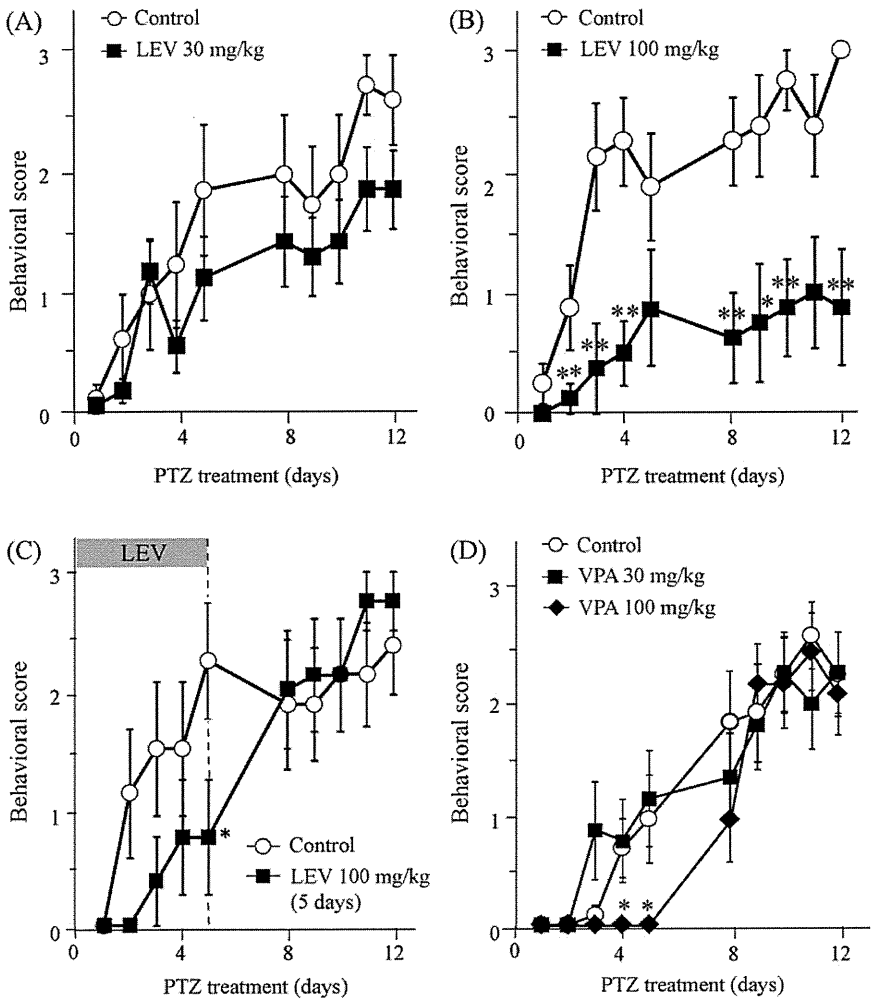

Figure 1 Effects of LEV and VPA on the development of PTZ kindling in mice. Animals were given 40 mg/kg (i.p.) of PTZ for 12 days along with the 30 min-pretreatment with LEV at 30 mg/kg (i.p.) (A), 100 mg/kg (i.p.) (B), or VPA (30 and 100 mg/kg, i.p.) (D). Withdrawal experiments after 5 days-treatment with LEV were also conducted (C). The severity of seizures was evaluated for 15 min immediately after the PTZ injection. Behavioral scores are expressed as the mean ± S.E.M., and analyzed by the Mann–Whitney test (two groups-comparison: A–C) or the Kruskal–Wallis test followed by the Steel–Dwass test (three groups-comparison: D). $^{*}P < 0.05$, $^{**}P < 0.01$, significantly different from the control values.

(i.p.), and these doses were repeatedly administered to the animals 30 min before PTZ (40 mg/kg, i.p.) injection for 12 days.

Repeated administration of sub-convulsive PTZ (40 mg/kg, i.p.) progressively increased seizure susceptibility in mice during the 12-day treatment (Fig. 1). The number of kindled animals, which consistently exhibited clonic seizures upon PTZ injection, increased and reached usually about 90%, 10–12 days after the treatment. However, LEV treatments at 30 and 100 mg/kg markedly inhibited the development of PTZ kindling in a dose-related manner (Fig. 1A and B). The incidence rate of PTZ seizure in animals treated with 100 mg/kg LEV was also suppressed to about 20% at Day 12. We also examined the withdrawal effects of LEV. LEV (100 mg/kg) was given daily along with PTZ for the first 5 days, and then, LEV was withdrawn. Under these conditions, LEV tended to prevent the development of PTZ kindling in the early stage, but these effects did not persist after cessation of the LEV administration (Fig. 1C).

In contrast to LEV, VPA at 30 and 100 mg/kg failed to prevent the development of PTZ kindling, although a slight reduction in the seizure scores was observed at the initial stage (~Day 5) of the treatment at 100 mg/kg (Fig. 1D). Incidence rates of PTZ-evoked seizures at the end of the treatment were comparable among groups treated with VPA at 30, 100 mg/kg or the vehicle (data not shown).

We next examined the anticonvulsive actions of LEV and VPA against PTZ seizures in fully kindled animals. In contrast to the naïve animals, the PTZ-kindled mice became responsive to LEV, in that, LEV at relatively low doses (3–30 mg/kg, i.p.) inhibited PTZ seizures in a dose-related manner (Table 1). The inhibitory effects of LEV were partial with a maximal inhibition rate of about 50% at 30 mg/kg (i.p.). On the other hand, VPA inhibited PTZ seizures in PTZ-kindled mice with potency (ED_{50} value = 227 mg/kg, i.p.) nearly identical to that in the naïve mice (Table 1).

Discussion

The present study demonstrated that repeated treatments with LEV effectively inhibited development and acquisition of PTZ kindling. In addition, LEV showed a significant ability to inhibit PTZ-evoked seizures specifically in kindled animals while being inactive in naïve animals. These characteristics are different from those of VPA, which failed to prevent the development of PTZ kindling and inhibited PTZ seizures in fully kindled and naïve animals at equipotent doses. Our results revealed that antiepileptic actions of LEV, which possess a novel action site SV2A, are uniquely different from those of conventional AEDs.

LEV inhibited the development and acquisition of PTZ kindling at a dose range which negligibly affected PTZ seizures in naïve animals. In contrast, the typical AED VPA at subanticonvulsive doses failed to prevent the development of PTZ kindling. Thus, LEV differs from VPA by dissociating the doses that provide acute seizure protection and prevention against the epileptogenic kindling process. The present results are consistent with previous findings (Löscher et al., 1998; Husum et al., 2004; Gu et al., 2004) that LEV inhibits the development of amygdala kindling in rats, and strongly suggest that that LEV possesses antiepileptogenic activity.

Previous study (Löscher et al., 1998) showed that inhibition of the development of amygdala kindling by LEV persisted at least for several days after cessation of the LEV treatment. We also showed that prophylactic LEV treatment given before seizure appearance could prevent the seizure development in a genetically defined spontaneous epileptic rat, SER (Yan et al., 2005). However, the antiepileptogenic action of LEV against PTZ kindling in this study disappeared rapidly after its withdrawal. The reasons for above differences remain uncertain, but this might be due to a relatively short period (5 days) of the LEV treatment before the withdrawal (cf. 3 weeks in Löscher's study). More extended treatment with LEV seems to be required to assess the sustained and/or prophylactic inhibition against PTZ kindling.

The present study confirmed that LEV is devoid of protective actions in acute convulsion models (e.g., maximal PTZ seizures), but it selectively inhibits seizures in kindled animals (Löscher and Hönack, 1993; Klitgaard et al., 1998; Bastlund et al., 2005). Since the kindling models are expected to be more predictive of partial seizures in man than acute models (Sato et al., 1990; Mody, 1993; Morimoto et al., 2004), the latter actions of LEV seem to reflect its broad-spectrum of efficacy in patients with partial epilepsy (Ben-Menachem and Falter, 2000; Cereghino et al., 2000; Glauser et al., 2006). We have recently shown that the hippocampal level of SV2A, a primary action site of LEV, was significantly elevated by PTZ kindling (Ohno et al., 2009). Since the anticonvulsive action of LEV has been shown to be closely associated with the expression level of SV2A in the brain (Kaminski et al., 2009), the seizure inhibition selectively observed in PTZ-kindled animals by LEV might be related to the kindling-induced increase in the hippocampal SV2A level.

In conclusion, the present study demonstrated that LEV contrasts VPA by preventing the development of PTZ kindling and inhibiting seizures selectively in kindled animals, supporting the notion that LEV possesses an antiepileptogenic potential. Nonetheless, we cannot completely deny a possibility that the differences in pharmacokinetic properties between two drugs (e.g., relatively short half-life of elimination for VPA) might influence upon those in their pharmacological actions. Further studies will be required to elucidate the mode and mechanism of the antiepileptogenic actions of LEV.

Acknowledgments

This work was partly supported by the Japan Epilepsy Research Foundation. We thank UCB Japan (Tokyo, Japan) for kindly donating a sample of LEV.

References

Bastlund, J.F., Berry, D., Watson, W.P., 2005. Pharmacological and histological characterisation of nicotine-kindled seizures in mice. Neuropharmacology 48, 975–983.

Ben-Menachem, E., Falter, U., European Levetiracetam Study Group, 2000. Efficacy and tolerability of levetiracetam 3000 mg/d in patients with refractory partial seizures: a multicenter, double-blind, responder-selected study evaluating monotherapy. Epilepsia 41, 1276–1283.

Bouwman, B.M., van Rijn, C.M., 2004. Effects of levetiracetam on spike and wave discharges in WAG/Rij rats. Seizure 13, 591–594.

Brandt, C., Glien, M., Gastens, A.M., Fedrowitz, M., Bethmann, K., Volk, H.A., Potschka, H., Löscher, W., 2007. Prophylactic treatment with levetiracetam after status epilepticus: lack of effect on epileptogenesis, neuronal damage, and behavioral alterations in rats. Neuropharmacology 53, 207–221.

Cereghino, J.J., Biton, V., Abou-Khalil, B., Dreifuss, F., Gauer, L.J., Leppik, I., 2000. Levetiracetam for partial seizures: results of a double-blind, randomized clinical trial. Neurology 55, 236–242.

Glauser, T.A., Ayala, R., Elterman, R.D., Mitchell, W.G., Van Orman, C.B., Gauer, L.J., Lu, Z., N159 Study Group, 2006. Double-blind placebo-controlled trial of adjunctive levetiracetam in pediatric partial seizures. Neurology 66, 1654–1660.

Gower, A.J., Hirsch, E., Boehrer, A., Noyer, M., Marescaux, C., 1995. Effects of levetiracetam, a novel antiepileptic drug, on convulsant activity in two genetic rat models of epilepsy. Epilepsy Res. 22, 207–213.

Gu, J., Lynch, B.A., Anderson, D., Klitgaard, H., Lu, S., Elashoff, M., Ebert, U., Potschka, H., Löscher, W., 2004. The antiepileptic drug levetiracetam selectively modifies kindling-induced alterations in gene expression in the temporal lobe of rats. Eur. J. Neurosci. 19, 334–345.

Husum, H., Bolwig, T.G., Sánchez, C., Mathé, A.A., Hansen, S.L., 2004. Levetiracetam prevents changes in levels of brain-derived neurotrophic factor and neuropeptide Y mRNA and of Y1- and Y5-like receptors in the hippocampus of rats undergoing amygdala kindling: implications for antiepileptogenic and mood-stabilizing properties. Epilepsy Behav. 5, 204–215.

Ji-qun, C., Ishihara, K., Nagayama, T., Serikawa, T., Sasa, M., 2005. Long-lasting antiepileptic effects of levetiracetam against epileptic seizures in the spontaneously epileptic rat (SER): differentiation of levetiracetam from conventional antiepileptic drugs. Epilepsia 46, 1362–1370.

Kaminski, R.M., Matagne, A., Leclercq, K., Gillard, M., Michel, P., Kenda, B., Talaga, P., Klitgaard, H., 2008. SV2A protein is a broad-spectrum anticonvulsant target: functional correlation between protein binding and seizure protection in models of both partial and generalized epilepsy. Neuropharmacology 54, 715–720.

Kaminski, R.M., Gillard, M., Leclercq, K., Hanon, E., Lorent, G., Dassesse, D., Matagne, A., Klitgaard, H., 2009. Proepilep-

tic phenotype of SV2A-deficient mice is associated with reduced anticonvulsant efficacy of Levetiracetam. Epilepsia 50, 1729–1740.

Klitgaard, H., Matagne, A., Gobert, J., Wülfert, E., 1998. Evidence for a unique profile of levetiracetam in rodent models of seizures and epilepsy. Eur. J. Pharmacol. 353, 191–206.

Löscher, W., Hönack, D., 1993. Profile of ucb L059, a novel anticonvulsant drug, in models of partial and generalized epilepsy in mice and rats. Eur. J. Pharmacol. 232, 147–158.

Löscher, W., Hönack, D., Rundfeldt, C., 1998. Antiepileptogenic effects of the novel anticonvulsant levetiracetam (ucb L059) in the kindling model of temporal lobe epilepsy. J. Pharmacol. Exp. Ther. 284, 474–479.

Lynch, B.A., Lambeng, N., Nocka, K., Kensel-Hammes, P., Bajjalieh, S.M., Matagne, A., Fuks, B., 2004. The synaptic vesicle protein SV2A is the binding site for the antiepileptic drug levetiracetam. Proc. Natl. Acad. Sci. U.S.A. 101, 9861–9866.

Matveeva, E.A., Vanaman, T.C., Whiteheart, S.W., Slevin, J.T., 2008. Levetiracetam prevents kindling-induced asymmetric accumulation of hippocampal 7S SNARE complexes. Epilepsia 49, 1749–1758.

Mody, I., 1993. The molecular basis of kindling. Brain Pathol. 3, 395–403.

Morimoto, K., Fahnestock, M., Racine, R.J., 2004. Kindling and status epilepticus models of epilepsy: rewiring the brain. Prog. Neurobiol. 73, 1–60.

Ohno, Y., Ishihara, S., Terada, R., Kikuta, M., Sofue, N., Kawai, Y., Serikawa, T., Sasa, M., 2009. Preferential increase in the hippocampal synaptic vesicle protein 2A (SV2A) by pentylenetetrazole kindling. Biochem. Biophys. Res. Commun. 390, 415–420.

Sasa, M., 2006. A new frontier in epilepsy: novel antiepileptogenic drugs. J. Pharmacol. Sci. 100, 487–494.

Sato, M., Racine, R.J., McIntyre, D.C., 1990. Kindling: basic mechanisms and clinical validity. Electroencephalogr. Clin. Neurophysiol. 76, 459–472.

Yan, H.D., Ji-qun, C., Ishihara, K., Nagayama, T., Serikawa, T., Sasa, M., 2005. Separation of antiepileptogenic and antiseizure effects of levetiracetam in the spontaneously epileptic rat (SER). Epilepsia 46, 1170–1177.

OPEN ACCESS Freely available online

PLoS one

Generation of Knockout Rats with X-Linked Severe Combined Immunodeficiency (X-SCID) Using Zinc-Finger Nucleases

Tomoji Mashimo[1]*, Akiko Takizawa[1], Birger Voigt[1], Kazuto Yoshimi[1], Hiroshi Hiai[2], Takashi Kuramoto[1], Tadao Serikawa[1]

1 Institute of Laboratory Animals, Graduate School of Medicine, Kyoto University, Kyoto, Japan, **2** Shiga Medical Center for Adult Disease, Moriyama, Japan

Abstract

Background: Although the rat is extensively used as a laboratory model, the inability to utilize germ line-competent rat embryonic stem (ES) cells has been a major drawback for studies that aim to elucidate gene functions. Recently, zinc-finger nucleases (ZFNs) were successfully used to create genome-specific double-stranded breaks and thereby induce targeted gene mutations in a wide variety of organisms including plants, drosophila, zebrafish, etc.

Methodology/Principal Findings: We report here on ZFN-induced gene targeting of the rat interleukin 2 receptor gamma (*Il2rg*) locus, where orthologous human and mouse mutations cause X-linked severe combined immune deficiency (X-SCID). Co-injection of mRNAs encoding custom-designed ZFNs into the pronucleus of fertilized oocytes yielded genetically modified offspring at rates greater than 20%, which possessed a wide variety of deletion/insertion mutations. ZFN-modified founders faithfully transmitted their genetic changes to the next generation along with the severe combined immune deficiency phenotype.

Conclusions and Significance: The efficient and rapid generation of gene knockout rats shows that using ZFN technology is a new strategy for creating gene-targeted rat models of human diseases. In addition, the X-SCID rats that were established in this study will be valuable *in vivo* tools for evaluating drug treatment or gene therapy as well as model systems for examining the treatment of xenotransplanted malignancies.

Citation: Mashimo T, Takizawa A, Voigt B, Yoshimi K, Hiai H, et al. (2010) Generation of Knockout Rats with X-Linked Severe Combined Immunodeficiency (X-SCID) Using Zinc-Finger Nucleases. PLoS ONE 5(1): e8870. doi:10.1371/journal.pone.0008870

Editor: Ellen A. A. Nollen, University Medical Center Groningen, Netherlands

Received November 12, 2009; **Accepted** January 4, 2010; **Published** January 25, 2010

Funding: This study was supported in part by a grant-in-aid for cancer research from the Ministry of Health, Labour, and Welfare. The funders had no role in study design, data collection and analysis, decision to publish, or preparation of the manuscript.

Competing Interests: The authors have declared that no competing interests exist.

* E-mail: tmashimo@anim.med.kyoto-u.ac.jp

Introduction

Although several strategies are available for producing a wide variety of genomic alterations in the mouse, the same cannot be said of the rat. Rat ES cells [1,2] and induced pluripotent stem cells (iPS) [3,4] are available, but the culture conditions for these cells and the methodology for inducing homologous recombination are imperfect [5]. Rat spermatogonial stem cells (SSC) have also been isolated and cultivated *in vitro* but their yield proved unsatisfactory in terms of their ability to undergo homologous recombination [6,7]. Besides these methods which are based on the *in vitro* genetic engineering of pluripotent stem cells, transposon-mediated mutagenesis [8] and N-ethyl-N-nitrosourea (ENU) mutagenesis [9,10] have been used with some success for producing mutations in the rat genome. We recently reported on a high-throughput gene-driven strategy which uses the mutagen ENU and the Mu-transposition reaction (MuT-POWER) to rapidly detect induced mutations. This was in addition to our investigation of intracytoplasmic sperm injection (ICSI) for recovering heterozygous genotypes of interest out of a large sperm cell repository [11,12]. However, even if a large number of mutant strains already exists or may potentially be available, targeted modification or disruption of specific DNA regions is difficult to achieve. Even in the case of our gene-driven strategy, X-linked mutations are impossible to obtain because of the breeding protocol which is used [11].

Recently, a novel gene-targeting technology which employs zinc-finger nucleases (ZFNs) has been proven to work successfully in plants, *Caenorhabditis elegans*, frogs, drosophila, zebrafish, and human ESCs and iPSCs [13,14,15]. ZFNs are chimeric proteins that consist of a specific DNA-binding domain which is made of tandem zinc finger-binding motifs that are fused to a non-specific cleavage domain of the restriction endonuclease *Fok*I. ZFNs can create site-specific double-stranded breaks which are repaired via non-homologous end joining (NHEJ), a process that results in the arbitrary addition or deletion of base pairs. Consequently, repair by NHEJ is mutagenic and results in a knockout. Recently, it was reported that a single injection of DNA or messenger RNA that encodes specific ZFNs into one-cell transgenic rat embryos that express GFP could lead to a high frequency of animals that do not express the transgenic marker as a consequence of homologous recombination at the GFP site [16]. Here, we report on an experiment that involved using ZFN technology. The aim of the experiment was to inactivate the gene that encodes the interleukin 2 receptor gamma (*Il2rg*), which is essential for signaling by interleukins such as IL-2, IL-4, IL-7, IL-9, IL-15, and IL-21. In

addition, the gene is involved in the X-linked form of severe combined immunodeficiency (X-SCID), one of the most common forms of human SCID [17,18]. A major motivation for performing this experiment was the observation that although SCID mouse animal models are the most commonly used in research on drug development, an X-SCID immunodeficient rat model would complement mouse models through the additional advantage of being employed for testing the pharmacodynamics and toxicity of potential therapeutic compounds. Following the results of research involving *Prkdc* SCID [19,20] and *Il2rg* X-SCID mice [21,22,23], *Il2rg* X-SCID rats should have a very low level of NK cell activity and thereby make xenotransplantation more successful.

Results

Injection of *Il2rg* ZFN-encoding mRNA into rat embryos

Of 443 ZFN-injected embryos, 230 (51.9%) were transferred into the oviducts of pseudopregnant female rats, and 54 (24.3%) of these embryos were successfully carried to term as shown in Figure 1a, b and Table 1. Sequence analysis of the ZFN target site of these 54 founder animals revealed that 5 males and 8 females (24.1%) carried a variety of mutations including from 3 to1,097 bp deletions and a 1 bp insertion in the region which overlapped the ZFN target site as seen in Figure 1c and Figure S1. Four out of five of the males carried different biallelic mutations at the *Il2rg* locus despite them only having one X chromosome. This suggests that mosaicism was induced by the ZFN treatment, a situation which is frequently observed in the DNA of transgenic founders. Three of the affected females had a monoallelic homozygous mutation, four had heterologous or mosaicism biallelic mutations, and the remainder had three different mosaic mutations. The normal F344-allele was not found in the affected founder animals. Most of these mutations were expressed as frameshifts or splicing errors and resulted in no or very little IL2RG mRNA being expressed as shown in Figure 1d probably due to nonsense-mediated decay. Western blotting with antibodies against the C-terminal domain of

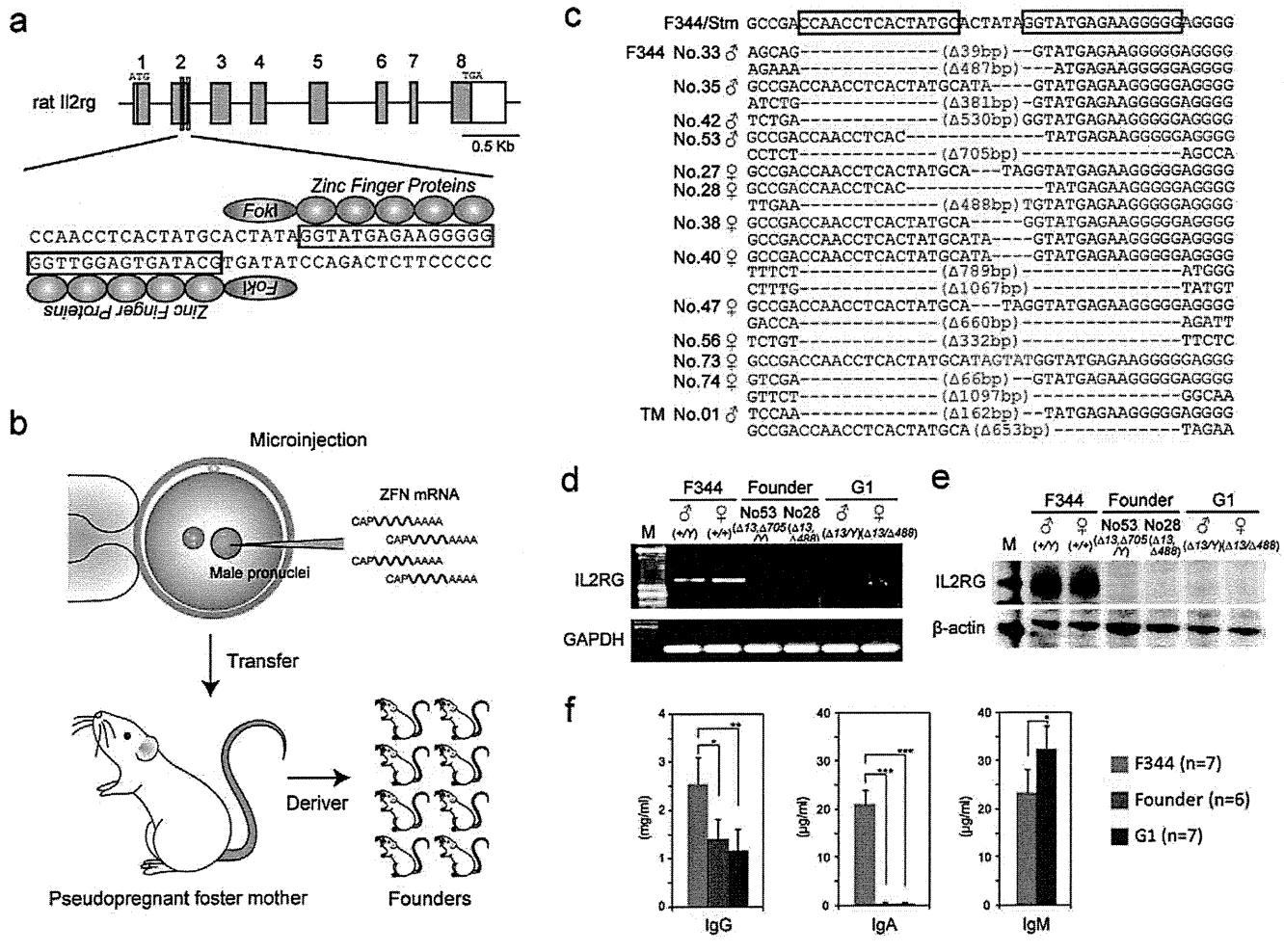

Figure 1 Injection of *Il2rg* ZFN-encoding mRNA into rat embryos induced targeted loss-of-function mutations. (a) Schematic representation of the rat *Il2rg* gene. Exons are represented as blue boxes. Regions used to design the ZFN templates are printed in red for the left ZFN and green for the right ZFN. The magnified views illustrate the binding sites for the ZFN pairs. Please see Figure S4 for further details. (b) Schematic representation of the method used for ZFN-targeted mutagenesis in rat embryos. (c) Sequencing assay for ZFN-induced mutations in the *Il2rg*-targeted region. Multiple deletions or insertions depicted using red dashes or letters, respectively, are aligned along the wild-type sequences shown on the top line. (d) RT-PCR analysis of IL2RG mRNA expression in the spleen of control F344, founder (G0), and G1 rats. GAPDH expression was used as an internal control. (e) Western blotting for IL2RG protein in the spleen of control F344, founder (G0), and G1 rats. β-actin was used as a loading control. (f) ELISA for serum IgG, IgA, and IgM levels in control F344, founder (G0), and G1 rats. *P<0.01, **P<0.001, and ***P<0.0001, indicated for each group in comparison with control F344 for independent sample Student t-tests.
doi:10.1371/journal.pone.0008870.g001

Table 1. Injection of ZFN-encoding mRNA into fertilized oocytes.

Strain	Oocyte state	Injected oocytes	Transferred oocytes (%)	Born (%)	Mutants (%)
F344/Stm	Fresh	234	32 (-)	♂2,♀5 (21.9)	♀2 (28.6)
	Cryopreserved[a]		57 (-)	♂8,♀10 (31.6)	♀2 (11.1)
	Fresh	182	129 (68.3)	♂16,♀11 (20.9)	♂4,♀4 (29.6)
TM/Kyo	Fresh	27	12 (44.4)	♂1,♀1 (16.7)	♂1 (50.0)
Total		**443**	**230 (51.9)**	**♂27,♀27 (24.3)**	**♂5,♀8 (24.1)**

[a]Injected oocytes were cultured in KRB overnight and cryopreserved at the two-cell stage.
doi:10.1371/journal.pone.0008870.t001

IL2RG did not reveal any protein in the founder animals as seen in Figure 1e.

To clarify whether the ZFNs only induced mutations in the targeted region, we checked 16 sites that showed a high rate of similarity with the targeted site at the sequence level with no more than 6 to 7 bp mismatches as illustrated in Table S1. Insertions or deletions were not observed at any of these off-target sites among the 13 ZFN-modified founders. This confirms that ZFNs can be reliably and efficiently used to produce mutant alleles at loci of interest. Although we cannot exclude the possibility that the ZFNs may have cleaved unknown off-target sites, such undesired mutations can subsequently be easily excluded from the genome of the carrier animals by backcrossing to the parental strain or another background strain.

Germ line transmission of ZFN-modified genetic changes

To assess the transmission of ZFN-modified genetic changes to the next generation, we crossed the founder animals with the background strain F344/Stm as depicted in Table S2. All 38 offspring consisting of 18 males and 20 females that were obtained from the founder females mated with the F344 males had one of the maternal mutations. This indicates that ZFN-induced mutations were faithfully transmitted through the germ line. In the offspring that were obtained from the founder males, there were two cases where only one of the paternal bialleles was transmitted or both alleles were transmitted. This suggests that mosaicism occurred not only in somatic cells but also in the germ line of the founder animals. PCR analysis of genomic DNA isolated from several types of tissues indicated that somatic mosaicism occurred in the progenitors but not in their offspring as shown in Figure S2.

We intercrossed the G0 founders to produce hemizygous males (*Il2rg*$^{-}$/*Y*) and homozygous females (*Il2rg*$^{-}$/*Il2rg*$^{-}$) for the ZFN-induced mutation listed in Table S3 to characterize the immunodeficient phenotypes of the X-SCID rats. The hemizygous males and homozygous females appeared normal at birth and developed well as shown in Figure 2a. RT-PCR and Western blot assays was performed on these G1 rats and the results showed a complete loss of expression of the *Il2rg* gene as detailed in Figures 1d, e. ELISA for serum immunoglobulin (Ig) levels revealed reduced IgG, diminished IgA, and increased IgM levels in the G1 rats as noted in Figure 1f.

Characterization of *Il2rg*-deficient X-SCID rats

Gross and microscopic analyses at five weeks of age showed that the X-SCID rats underwent abnormal lymphoid development as depicted in Figure 2. The thymus of X-SCID rats was extremely hypoplastic as seen in Figure 2b and consisted of an epithelial rudiment without any lymphocytes as seen in Figure 2d. The spleen was moderately decreased in size as noted in Figure 2c, and the white pulp was severely hypoplastic and the red pulp contained myeloid cells as shown in Figure 2f. Peripheral lymph nodes and Peyer's patches were not identified by necropscopy. In the peripheral blood (PB) profiles, the numbers of white blood cells (WBCs) was reduced compared to those of control rats as detailed in Table S4. Differential counts of WBCs showed a dramatic decrease in leukocytes in the X-SCID rats (Table S5). Flow cytometry analysis of cell populations isolated from PB, bone marrow (BM), and the spleen also revealed a dramatic decrease in the number of the lymphocytes as seen in Figure 2h and Figure S3. The number of $CD4^{-}CD8^{+}$ T-cells was markedly diminished and the number of $CD4^{+}CD8^{-}$ T-cells was decreased although some cells were present in PB, BM and the spleen. The numbers of $CD3^{-}CD45RA^{+}$ B-cells and $CD3^{-}CD161a^{+}$ NK cells were markedly diminished in PB and BM, but some cells were present in the spleen. Heterozygous females exhibited normal lymphoid development and were indistinguishable from normal control females (data not shown).

Xenotransplantation of human tumor cells

These immunodeficient phenotypes of the X-SCID rats were very similar to those of the previously reported X-SCID mice and were characterized by a nearly complete lack of T-cells, B-cells and NK cells [21,22,23]. Since X-SCID mice cannot reject transplanted tissues from other species including humans, we tested *Il2rg*-deficient rats as a host for xenotransplantation of human ovarian cancer tumor cells. All X-SCID rats developed tumors within 14 days after injection of the cells (6/6, 100%), while control F344 rats showed no tumor growth (0/6, 0%) as seen in Figure 3a, b. The tumors were confirmed by histological analysis as depicted in Figure 3c and by PCR with primers that were used to amplify the human MHC class II DQB2 region (data not shown). These observations illustrate the impaired immune system function of X-SCID rats and suggest that the animals may be important models for cancer and transplantation research.

Discussion

In this study, we proved that targeted gene disruption using ZFN technology works well and provides for several advantages and possibilities when used in rats. First and foremost, knockout rats can be created in a four- to six-month time frame and with high efficiency at more than 20%. This is more favorable than the ES cell-based method for mice that usually takes 12–18 months. Given the high rate of germ line transmission, preliminary phenotypic analysis can be performed on G1 animals after intercrossing the initial G0 founders, thereby saving time and effort. Second, gene-targeting with ZFNs does not seem to be strain-dependent (unpublished data) and accordingly can be performed with any inbred strain. This is of great advantage

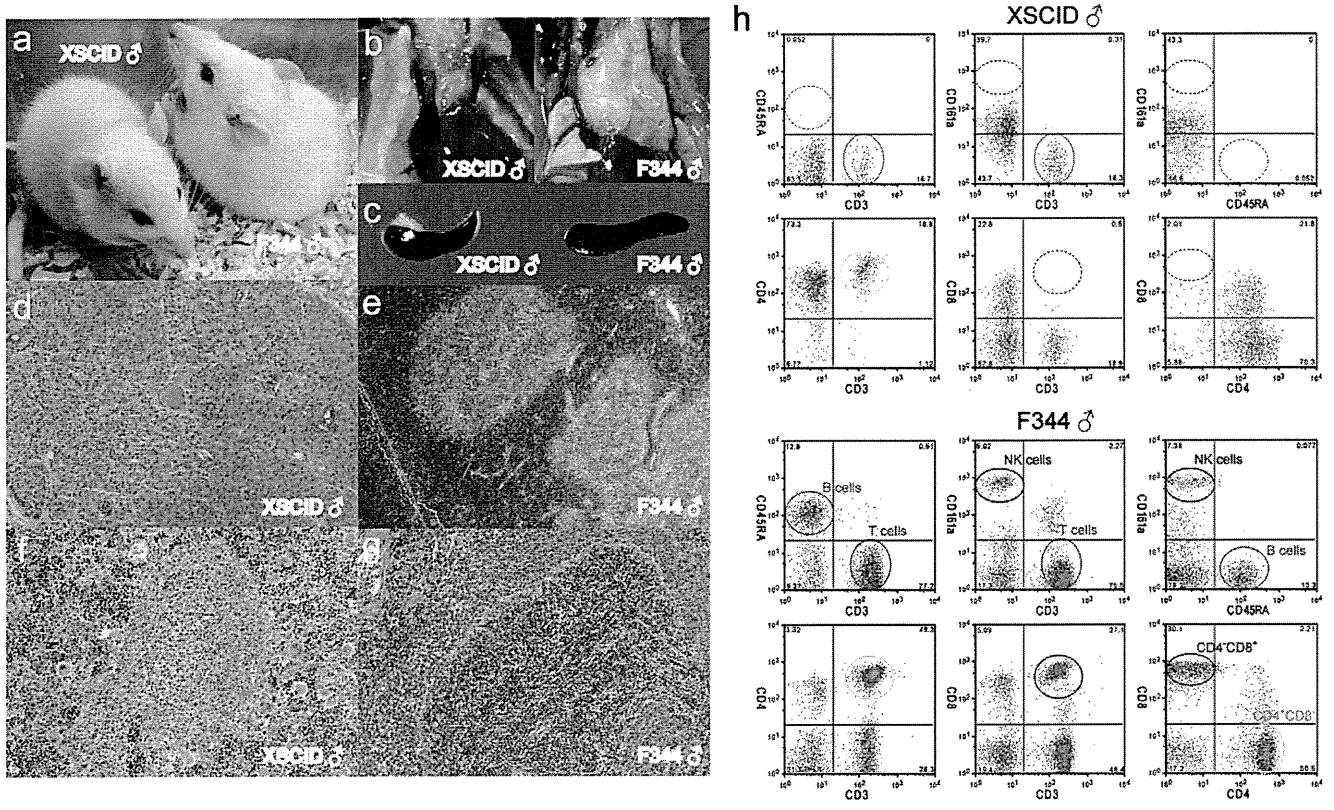

Figure 2 Abnormal lymphoid development in X-SCID rats. (a) Photograph of five week-old male X-SCID (*Il2rg*$^{-}$/*Y*) and F344 (+/*Y*) rats. (b) Thymus of X-SCID and F344 rats. (c) Spleen of X-SCID and F344 rats. (d, e) Histological analysis of the thymus of X-SCID (X40) and F344 (X40) rats. The thymus of the X-SCID rat was severely hypoplastic and consisted of an epithelial cell sheet. (f, g) Histological analysis of the spleen of X-SCID (X100) and F344 (X100) rats. In the X-SCID spleen, the white pulp was virtually devoid of lymphocytes and the red pulp was occupied by a variety of myeloid elements. (h) Dot plots representing CD3, CD45RA and CD161a for differentiation of T-, B- and NK cell sub-populations, and CD3, CD4 and CD8 for demarcation of T-cell sub-populations in peripheral blood lymphocyte cells. The numbers shown in the quadrants are mean percentages. The circled areas indicate cell populations that are referred to in the text.
doi:10.1371/journal.pone.0008870.g002

since other techniques like ENU mutagenesis differ in their efficiency when used with different strains. This provides a straight forward strategy for directly employing targeted gene disruption in the existing strain, thereby bypassing tedious and time-consuming backcrossing steps that generally take two to three years to complete. Third, ZFNs can be used to induce a wide variety of allelic changes covering small or wide deletions or insertions. They may be used to produce frameshifts or small in-frame deletions such as the 3-bp deletion that we observed. Given the reports on successful ZFN-targeted gene modification or correction by homologous recombination in mammalian cell cultures [15,24,25], it should be feasible to archive targeted knock-in technologies that have thus been far inaccessible without rat ES cells. Finally, since ZFN technology does not rely on using species-specific embryonic stem cell lines, it should be possible to adapt it to other mammalian species such as pigs, cattle, and monkeys, where it is possible to harvest and manipulate fertilized embryos.

The X-SCID rats established in this study provide not only a valuable *in vivo* model for evaluating drug treatment or gene therapy approaches, but also a system for assaying novel anticarcinogenic effects on transplanted malignancies. There is a growing need for animal models with which to carry out *in vivo* studies using human cells, tissues or organs as chimeras such as humanized models [26,27,28]. X-SCID and SCID mice homozygous for *Il2rg*- and *Prkdc*- alleles with a non-obese diabetic background are a powerful tool for the xenotransplantation of human tissues or potentially human ES/iPS cells. This could lead to advances in our understanding of human hematopoiesis, immunology, cancer biology, infectious diseases, and regenerative medicine [29,30,31]. Humanized rats, if generated by ZFN technology, could be powerful tools for pre-clinical testing during drug development and be better models in various fields of translational research.

Materials and Methods

Animals

All animal care and experiments conformed to the Guidelines for Animal Experiments of Kyoto University, and were approved by the Animal Research Committee of Kyoto University. F344-*Il2rg*^{tm1Kyo} X-SCID rats are deposited at the National Bio Resource Project for the Rat in Japan (www.anim.med.kyoto-u.ac.jp/nbr).

ZFN constructs

Custom-designed ZFNs plasmids for the rat *Il2rg* gene were obtained from Sigma-Aldrich. The design, cloning, and validation of the ZFNs was performed by Sigma-Aldrich [32]. ZFN design involved using an archive of pre-validated two-finger and one-finger modules [32,33]. The target region was scanned for positions where modules exist in the archive. This allowed the fusion of two or three such molecules to generate a five-finger

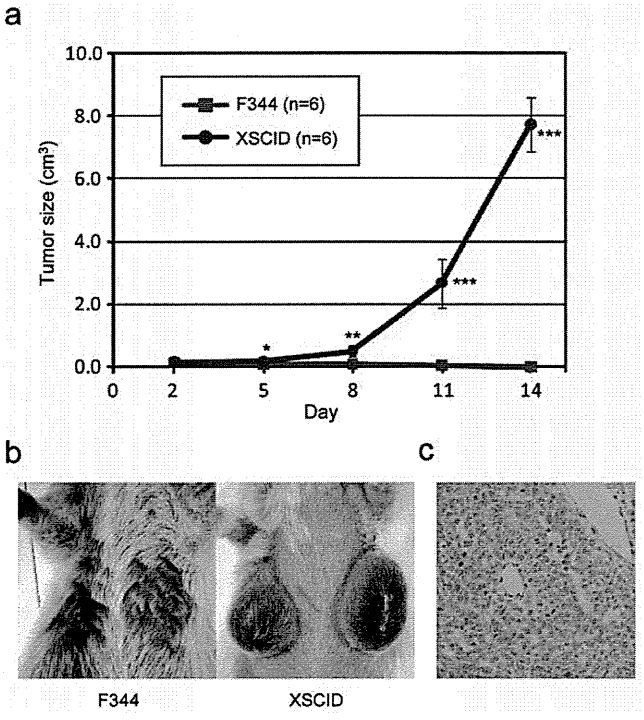

Figure 3 Tumor development from the xenotransplantation of human ovarian cancer cells. (a) Growth curve of tumor development after subcutaneous injection of A2780 human ovarian cancer cells in F344 and X-SCID rats. *P<0.01, **P<0.001, and ***P<0.0001, indicated in comparison with control F344. (b) The tumors became large and grew quickly about 11 days after injection in X-SCID rats but not in F344 rats. (c) Histology of the xenotransplanted tumors that formed in X-SCID rats (X400). No lymphocytic infiltration was detected in the tumors.
doi:10.1371/journal.pone.0008870.g003

protein that recognizes a 15 bp site on the top strand and the fusion of two to three different modules that recognize a 15 bp site on the bottom strand that lies 5–6 bp away. Measurements of ZFNs for gene disruption activity were performed using the Surveyor endonuclease (CEL-1) assay as described elsewhere [34]. Final candidate ZFNs were designed to recognize a site within the boundary between exon 2 and intron 2 of the *Il2rg* gene as shown in Figure S4.

Microinjection of ZFN mRNA

To prepare ZFN mRNA, ZFN-encoding expression plasmids were linearized with *Xho*I and extracted with phenol-chloroform by the standard method. Messenger RNA was transcribed *in vitro* using a MessageMax^{TM} T7 mRNA transcription kit (Epicentre) and polyadenylated using a A-Plus^{TM} Poly(A) polymerase tailing kit (Epicentre). The resulting mRNA was purified using a MEGAClear^{TM} kit (Epicentre) and finally resuspended in RNase-free water at 10 ng/μl for each ZFN. Approximately 2–3 pL of capped mRNA were injected into the male pronuclei of zygotes by the same method that was used to microinject DNA. Pronuclear stage embryos were collected from F344/Stm and TM/Kyo females six weeks of age that had been super-ovulated by injecting them with eCG (Serotropin, Asuka Pharmaceutical Co.) and hCG (Gonatropin, Asuka Pharmaceutical Co.). They were mated with males of the same respective strain. The mRNA solution was injected and embryos were cultured in KRB at 37.5°C with 5% CO_2 and 95% humidified air to promote their recovery. The embryos that survived were transferred to the oviduct of pseudopregnant females (Crlj:WI, 8–12wks).

Analysis of genome editing at ZFN target sites

Genomic DNA was extracted from the tail, brain, heart, and liver using a GENEXTRACTOR TA-100 automatic DNA purification system (Takara). PCR for each was carried out in a total volume of 15 μl under the following conditions for 35 cycles: 94°C for 3 min for 1 cycle, 94°C for 30 sec, 60°C for 30 sec, and 72°C for 1 min. The final reaction mixture for each contained 100 ng of genomic DNA, 200 μM of each dNTP, 1.0 mM $MgCl_2$, 0.66 μM of each primer, and 0.4 U of Taq DNA polymerase (GibcoBRL).

For editing the ZFN cleavage site in the genome at the *Il2rg* locus, three primer sets were designed to amplify small 292-bp, middle 1509-bp, and large 3158-bp fragments as shown in Figure S4. The PCR products were directly sequenced using the BigDye terminator v3.1 cycle sequencing mix and the standard protocol for an Applied Biosystems 3130 DNA Sequencer. The products were also subcloned into the pCR4-TOPO vector (Invitrogen), and plasmid DNA was prepared and sequenced on a 3130 DNA Sequencer. All new sequence data is deposited in GenBank (GU294902-GU294925).

Off-target site analysis

Off-target sites with the highest degree of similarity were identified by searching the rat genome (RGSCv3.4) for matches with the consensus sequence of each ZFP with appropriate spacing of 5–6 bp. A list of these target sites is provided in Supplementary Table 1. PCR primers were designed to flank the off-target sites as detailed in Table S6. Reactions were performed for the founder animals and the PCR products were directly sequenced on the 3130 DNA Sequencer.

RT-PCR and Western blotting

Total RNA was extracted using Isogen reagent (Nippon Gene) from the spleen of five week-old rats. First strand cDNA was synthesized from 5 μg of total RNA that had been treated using DNase by using the oligo(dT)12–18 primer and SuperscriptII reverse transcriptase (Invitrogen). PCR was performed with the primers for *Il2rg* described in Figure S4 and with the *Gapdh* 5′-GGCACAGTCAAGGCTGAGAATG-3′ and 5′-ATGGTGGT-GAAGACGCCAGTA-3′. Western blotting was carried out using the cell lysates from the spleens of five week-old rats by the standard method. Signals were detected with antibodies against rat IL2RG (M-20, Santa Cruz Biotechnology) and β-actin (AC-40, Sigma Aldrich).

Immunofluorescence and histological analyses

Complete necroscopy examinations were performed on five week-old *Il2rg*-deficient and wild-type male and female rats. Peripheral blood specimens were collected from the caudal vena cava. Serum immunoglobulin (Ig) levels were measured by enzyme-linked immunosorbent assay (ELISA) using Rat IgG, IgA and IgM ELISA Quantitation kits (Bethyl Laboratories). Blood parameters for a complete blood cell count, a WBC differential, and a reticulocyte count were measured using ADVIA 2120 flow cytometry (Block Scientific). For histopathology, tissues were fixed in Bouin's fluid and embedded in paraffin. The embedded tissues were then sectioned at 5–7 μm thickness at room temperature and stained with hematoxylin and eosin to permit evaluation by light microscopy.

Flow cytometric analyses of cell populations isolated from bone marrow, the spleen and peripheral blood were carried out using IOTest Anti-Rat CD3-FITC/CD45RA-PC7/CD161a-APC (Beckman Coulter) to differentiate T-, B- and NKcell subpopulations and IOTest Anti-Rat CD3-FITC/CD4-PC7/CD8-APC (Beckman Coulter) to enumerate T-cell sub-populations. Anti-CD45 monoclonal antibodies (Beckman Coulter) were used for the intracellular staining of lymphocytes. Mouse IgM, IgG1 and IgG2a antibodies (Beckman Coulter) were used as isotype-matched controls. The cell samples were treated with FcR-blocking reagent (Miltenyi Biotec) for 10 minutes, stained with the fluorochrome-conjugated antibodies for 30 minutes, and washed three times with PBS/10% FCS. Stained cell samples were analyzed with a four-color FACS flow cytometer (FACSCalibur, Becton Dickinson) using CellQuest software (Becton Dickinson).

Tumor cell xenotransplantation

The human ovarian cancer cell line A2780 was purchased from the European Collection of Cell Cultures (ECACC). Cells were cultured in RPMI1640 medium (GIBCO) with 10% heat-inactivated FBS (Hyclone). Subcutaneous injections of 2×10^5 A2780 cells with Matrigel (Becton Dickinson) were performed on five week-old female rats. Tumors were measured by length (a) and width (b) in millimeters using calipers, and tumor volumes (V) were calculated according to the relationship $V = ab^2/2$, where a was the longer of the two measurements. Human-specific PCR primers were designed to amplify major histocompatibility complex class II DQ beta 2 (HLA-DQB2) at exon 4 as follows: 5′-CCTAGG-GTGGTCAGACTGGA-3′ and 5′-AAAATCCCCCAAAACA-AAGG-3′.

Supporting Information

Figure S1 PCR analysis of 13 mutant founders for the zinc-finger nuclease (ZFN) target site. For the analysis of the ZFN target site at the *Il2rg* locus, three primer sets were used to amplify small (a, 292-bp), middle (b, 1509-bp), and large (c, 3158-bp) fragments for PCR. See Figure S4 for further details. PCR fragments were electrophoresed through a 1-4% agarose gel. M: DNA molecular weight marker ϕX174-*Hae*III digest.
Found at: doi:10.1371/journal.pone.0008870.s001 (9.19 MB TIF)

Figure S2 PCR analysis of genomic DNA isolated from several tissues. Three primer sets were used to amplify small (a, 292-bp), middle (b, 1509-bp), and large (c, 3158-bp) fragments for PCR. See Figure S4 for further details. Genomic DNA (T: tail, B: brain, H: heart, L: liver) was used as a template for PCR in zinc-finger nuclease-modified founders (numbers 28, 35, 40, and 53) and G1 rats. PCR fragments were electrophoresed through a 1–4% agarose gel. M: DNA molecular weight marker ϕX174-*Hae*III digest or Lambda DNA-*Hind*III digest.
Found at: doi:10.1371/journal.pone.0008870.s002 (6.28 MB TIF)

Figure S3 Flow cytometric analysis of bone marrow lymphocyte cells (a) and spleen lymphocyte cells (b) from five-week-old F344 and X-SCID rats. Dot plots represent CD3, CD45RA, and CD161a for discrimination of T-, B-, and NK cell subpopulations; and CD3, CD4, and CD8 for demarcation of T cell subpopulations. The numbers shown in quadrants are mean percentages. Circled areas indicate cell populations referred to in the text.
Found at: doi:10.1371/journal.pone.0008870.s003 (6.66 MB TIF)

Figure S4 Zinc-finger nuclease pairs designed against the *Il2rg* locus and primer sequences used for PCR analysis for the *Il2rg* gene. Each exon is underlined. The start codon is indicated by a red box. The three primer sets (small, middle, and large) used for the PCR analysis of *Il2rg* are shown by boxes. Primers used for the RT-PCR are shown as cDNA.
Found at: doi:10.1371/journal.pone.0008870.s004 (3.32 MB TIF)

Table S1 Potential zinc-finger nuclease off-target sites.
Found at: doi:10.1371/journal.pone.0008870.s005 (0.14 MB DOC)

Table S2 Backcrossing of zinc-finger nuclease-modified founders to F344/Stm rats.
Found at: doi:10.1371/journal.pone.0008870.s006 (0.16 MB DOC)

Table S3 Intercrossing of zinc-finger nuclease-modified founders between males and females.
Found at: doi:10.1371/journal.pone.0008870.s007 (0.08 MB DOC)

Table S4 Peripheral blood profiles of *Il2rg*-deficient (X-SCID) rats.
Found at: doi:10.1371/journal.pone.0008870.s008 (0.09 MB DOC)

Table S5 Differential counts of the white blood cells of *Il2rg*-deficient (X-SCID) rats.
Found at: doi:10.1371/journal.pone.0008870.s009 (0.07 MB DOC)

Table S6 Primer sequences for zinc-finger nuclease off-target analysis.
Found at: doi:10.1371/journal.pone.0008870.s010 (0.14 MB DOC)

Acknowledgments

This study was supported in part by a Grant-in-aid for Cancer Research from the Ministry of Health, Labour and Welfare. We thank JL Guénet for critical discussion, and Y Kunihiro, F Tagami, and S Ishida for their assistance with the experiment.

Author Contributions

Conceived and designed the experiments: TM BV TS. Performed the experiments: TM AT KY HH TK. Analyzed the data: TM. Wrote the paper: TM.

References

1. Li P, Tong C, Mehrian-Shai R, Jia L, Wu N, et al. (2008) Germline competent embryonic stem cells derived from rat blastocysts. Cell 135: 1299–1310.
2. Buehr M, Meek S, Blair K, Yang J, Ure J, et al. (2008) Capture of authentic embryonic stem cells from rat blastocysts. Cell 135: 1287–1298.
3. Liao J, Cui C, Chen S, Ren J, Chen J, et al. (2009) Generation of induced pluripotent stem cell lines from adult rat cells. Cell Stem Cell 4: 11–15.
4. Li W, Wei W, Zhu S, Zhu J, Shi Y, et al. (2009) Generation of rat and human induced pluripotent stem cells by combining genetic reprogramming and chemical inhibitors. Cell Stem Cell 4: 16–19.
5. Voigt B, Serikawa T (2009) Pluripotent stem cells and other technologies will eventually open the door for straightforward gene targeting in the rat. Dis Model Mech 2: 341–343.
6. Ryu BY, Kubota H, Avarbock MR, Brinster RL (2005) Conservation of spermatogonial stem cell self-renewal signaling between mouse and rat. Proc Natl Acad Sci U S A 102: 14302–14307.
7. Shinohara T, Kato M, Takehashi M, Lee J, Chuma S, et al. (2006) Rats produced by interspecies spermatogonial transplantation in mice and in vitro microinsemination. Proc Natl Acad Sci U S A 103: 13624–13628.

8. Kitada K, Ishishita S, Tosaka K, Takahashi R, Ueda M, et al. (2007) Transposon-tagged mutagenesis in the rat. Nat Methods 4: 131–133.
9. Zan Y, Haag JD, Chen KS, Shepel LA, Wigington D, et al. (2003) Production of knockout rats using ENU mutagenesis and a yeast-based screening assay. Nat Biotechnol 21: 645–651.
10. Smits BM, Mudde JB, van de Belt J, Verheul M, Olivier J, et al. (2006) Generation of gene knockouts and mutant models in the laboratory rat by ENU-driven target-selected mutagenesis. Pharmacogenet Genomics 16: 159–169.
11. Mashimo T, Yanagihara K, Tokuda S, Voigt B, Takizawa A, et al. (2008) An ENU-induced mutant archive for gene targeting in rats. Nat Genet 40: 514–515.
12. Yoshimi K, Tanaka T, Takizawa A, Kato M, Hirabayashi M, et al. (2009) Enhanced colitis-associated colon carcinogenesis in a novel Apc mutant rat. Cancer Sci.
13. Porteus MH, Carroll D (2005) Gene targeting using zinc finger nucleases. Nat Biotechnol 23: 967–973.
14. Wu J, Kandavelou K, Chandrasegaran S (2007) Custom-designed zinc finger nucleases: what is next? Cell Mol Life Sci 64: 2933–2944.
15. Hockemeyer D, Soldner F, Beard C, Gao Q, Mitalipova M, et al. (2009) Efficient targeting of expressed and silent genes in human ESCs and iPSCs using zinc-finger nucleases. Nat Biotechnol 27: 851–857.
16. Geurts AM, Cost GJ, Freyvert Y, Zeitler B, Miller JC, et al. (2009) Knockout rats via embryo microinjection of zinc-finger nucleases. Science 325: 433.
17. Noguchi M, Yi H, Rosenblatt HM, Filipovich AH, Adelstein S, et al. (1993) Interleukin-2 receptor gamma chain mutation results in X-linked severe combined immunodeficiency in humans. Cell 73: 147–157.
18. Leonard WJ (2001) Cytokines and immunodeficiency diseases. Nat Rev Immunol 1: 200–208.
19. Blunt T, Finnie NJ, Taccioli GE, Smith GC, Demengeot J, et al. (1995) Defective DNA-dependent protein kinase activity is linked to V(D)J recombination and DNA repair defects associated with the murine scid mutation. Cell 80: 813–823.
20. Kirchgessner CU, Patil CK, Evans JW, Cuomo CA, Fried LM, et al. (1995) DNA-dependent kinase (p350) as a candidate gene for the murine SCID defect. Science 267: 1178–1183.
21. Cao X, Shores EW, Hu-Li J, Anver MR, Kelsall BL, et al. (1995) Defective lymphoid development in mice lacking expression of the common cytokine receptor gamma chain. Immunity 2: 223–238.
22. DiSanto JP, Muller W, Guy-Grand D, Fischer A, Rajewsky K (1995) Lymphoid development in mice with a targeted deletion of the interleukin 2 receptor gamma chain. Proc Natl Acad Sci U S A 92: 377–381.
23. Ohbo K, Suda T, Hashiyama M, Mantani A, Ikebe M, et al. (1996) Modulation of hematopoiesis in mice with a truncated mutant of the interleukin-2 receptor gamma chain. Blood 87: 956–967.
24. Urnov FD, Miller JC, Lee YL, Beausejour CM, Rock JM, et al. (2005) Highly efficient endogenous human gene correction using designed zinc-finger nucleases. Nature 435: 646–651.
25. Kandavelou K, Ramalingam S, London V, Mani M, Wu J, et al. (2009) Targeted manipulation of mammalian genomes using designed zinc finger nucleases. Biochem Biophys Res Commun 388: 56–61.
26. Dao MA, Tsark E, Nolta JA (1999) Animal xenograft models for evaluation of gene transfer into human hematopoietic stem cells. Curr Opin Mol Ther 1: 553–557.
27. Thomsen M, Yacoub-Youssef H, Marcheix B (2005) Reconstitution of a human immune system in immunodeficient mice: models of human alloreaction in vivo. Tissue Antigens 66: 73–82.
28. Shultz LD, Ishikawa F, Greiner DL (2007) Humanized mice in translational biomedical research. Nat Rev Immunol 7: 118–130.
29. Ito M, Kobayashi K, Nakahata T (2008) NOD/Shi-scid IL2rgamma(null) (NOG) mice more appropriate for humanized mouse models. Curr Top Microbiol Immunol 324: 53–76.
30. Quintana E, Shackleton M, Sabel MS, Fullen DR, Johnson TM, et al. (2008) Efficient tumour formation by single human melanoma cells. Nature 456: 593–598.
31. Machida K, Suemizu H, Kawai K, Ishikawa T, Sawada R, et al. (2009) Higher susceptibility of NOG mice to xenotransplanted tumors. J Toxicol Sci 34: 123–127.
32. Doyon Y, McCammon JM, Miller JC, Faraji F, Ngo C, et al. (2008) Heritable targeted gene disruption in zebrafish using designed zinc-finger nucleases. Nat Biotechnol 26: 702–708.
33. Santiago Y, Chan E, Liu PQ, Orlando S, Zhang L, et al. (2008) Targeted gene knockout in mammalian cells by using engineered zinc-finger nucleases. Proc Natl Acad Sci U S A 105: 5809–5814.
34. Miller JC, Holmes MC, Wang J, Guschin DY, Lee YL, et al. (2007) An improved zinc-finger nuclease architecture for highly specific genome editing. Nat Biotechnol 25: 778–785.